AGU ADVANCING EARTH AND SPACE SCIENCE

Earth and Space Science

RESEARCH ARTICLE
10.1029/2021EA002190

Observational Investigation of the Low-Level Jets in the Metropolitan Region of São Paulo, Brazil

Maciel Piñero Sánchez[1], Amauri Pereira de Oliveira[1], Ramón Pérez Varona[2], Janet Valdés Tito[1], Georgia Codato[1], Rita Yuri Ynoue[1], Flávia Noronha Dutra Ribeiro[3], Edson Pereira Marques Filho[4], and Lucas Cardoso da Silveira[1]

[1]Department of Atmospheric Sciences, Institute of Astronomy, Geophysics and Atmospheric Sciences, University of São Paulo, São Paulo, Brazil, [2]Department of Experimental Physics, Institute of Physics, University of São Paulo, São Paulo, Brazil, [3]School of Arts, Sciences and Humanities, University of São Paulo, São Paulo, Brazil, [4]Interdisciplinary Center for Energy and Environment, Federal University of Bahia, Salvador, Brazil

Key Points:

- The low-level jet (LLJ) is a remarkable robust feature of metropolitan region of São Paulo climate, occurring in more than 77% of time
- They occur during nighttime, under less disturbed synoptic conditions and more often in association to sea-breeze circulation
- Most of LLJ display inertial oscillation and are correlated with urban heat island, surface inversion layer, and air pollution

Supporting Information:

Supporting Information may be found in the online version of this article.

Correspondence to:

A. Pereira de Oliveira,
apdolive@usp.br

Citation:

Sánchez, M. P., Oliveira, A.P., Varona, R. P., Tito, J. V., Codato, G., Ynoue, R. Y., et al. (2022). Observational investigation of the low-level jets in the metropolitan region of São Paulo, Brazil. *Earth and Space Science*, *9*, e2021EA002190. https://doi.org/10.1029/2021EA002190

Received 22 DEC 2021
Accepted 29 AUG 2022
Corrected 19 OCT 2022

This article was corrected on 19 OCT 2022. See the end of the full text for details.

Author Contributions:

Conceptualization: Maciel Piñero Sánchez, Amauri Pereira de Oliveira, Flávia Noronha Dutra Ribeiro
Data curation: Georgia Codato

Abstract The main features of low-level jet (LLJ) in the metropolitan region of São Paulo (MRSP), Brazil, are assessed using rawinsondes carried out: (a) every 3-hr during 10-consecutive days in summer and winter field campaigns of the MCITY BRAZIL Project in 2013, (b) at 0900 and 2100 local time, from September 2009 to August 2013. These observations indicate that the LLJ is a typical feature of the MRSP, observed in 85% of the 20 days of the field-campaigns and 77.6% of the 1,446 days of regular rawinsonde period. The fine temporal and spatial resolution soundings indicate that most of the LLJs occur during nighttime and early in the morning, with mean intensity of 8.5 ± 0.3 m s^{-1}, height of 539 ± 26 m, and mostly (52.5%) from east and north. The coarse resolution soundings indicate the LLJ display a seasonal variation with maximum intensity in October (8.6 ± 0.3 m s^{-1}) and a minimum in February (7.1 ± 0.2 m s^{-1}), a maximum height in March (703 ± 151 m) and a minimum in June (577 ± 151 m). During MCITY campaigns about 76.4% of LLJ events show inertial oscillation and 35.3% of them are combined with sea breeze. Only 17.6% of LLJ events are associated with cold fronts and post-frontal high pressure system. The urban heat island intensity, surface inversion layer strength, particulate matter 2.5 and carbon monoxide concentrations are negatively correlated with the LLJ intensity, suggesting the jet-induced turbulent mixing may contribute to reduce them.

1. Introduction

During the night is common to observe in the vertical wind profile a maximum around the top of the surface inversion layer (SIL). Known as low-level jet (LLJ), it occurs most often between 100 and 500 m above the surface, under clear-sky conditions and without significant synoptic disturbances. Under these conditions, over land the nighttime surface radiational cooling strengthens the SIL intensity reducing turbulent friction and, as consequence, the flow above of the SIL top speeds up generating a relative maximum in the vertical wind profile (Baas et al., 2009; Barlow, 2014; Blackadar, 1957; Stull, 1988; Van de Wiel et al., 2010; Wei et al., 2013).

LLJ intensity and height are linked to the vertical distribution of the ageostrophic wind component as daytime convective turbulent mixing dyes out at the end of the afternoon. Therefore, the nighttime evolution of the LLJ depends also on the turbulence intensity of the previous daytime-convective boundary layer, varying according to the baroclinicity induced by land-ocean, soil moisture contrasts, land use and topography (Karam, 2002; Klein et al., 2016; Stull, 1988). First proposed by Blackadar (1957), the inertial oscillation mechanism has been used to explain LLJs formation, by formalizing a theoretical framework linking LLJ to time evolution of both nocturnal-stable and daytime-convective boundary layers (Karam, 2002; Karipot et al., 2009; Van de Wiel et al., 2010). Nevertheless, according to Lundquist (2003) and Kallistratova and Kouznetsov (2012), LLJs induced by inertial oscillation are not as frequent as initially thought. Indeed, observations indicate that LLJs are generated and sustained by baroclinicity induced by land-ocean differential surface heating in coastal regions (Kutsher et al., 2012; Parish, 2000; Wei et al., 2013), synoptic scale systems (Whiteman et al., 1997), such as Cold Front (CF), differential heating induced by sloping terrain (Holton, 1967; Ruchith & Raj, 2015; Whiteman et al., 1997), and by mechanical effects associated to topography such as mountain speeding up and along-valley channeling (Li & Chen, 1998; Parish, 1982).

The LLJs have been observed in different parts of the world, more frequently in the Great Plains, USA (Banta et al., 2002; Berg et al., 2015; Du et al., 2014; Klein et al., 2016; Lundquist & Mirocha, 2008; Parish, 2017; Shapiro

Formal analysis: Maciel Piñero Sánchez, Amauri Pereira de Oliveira, Rita Yuri Ynoue
Investigation: Maciel Piñero Sánchez, Amauri Pereira de Oliveira, Janet Valdés Tito, Flávia Noronha Dutra Ribeiro, Edson Pereira Marques Filho, Lucas Cardoso da Silveira
Methodology: Maciel Piñero Sánchez, Ramón Pérez Varona, Flávia Noronha Dutra Ribeiro
Project Administration: Georgia Codato, Edson Pereira Marques Filho
Software: Ramón Pérez Varona, Rita Yuri Ynoue
Supervision: Amauri Pereira de Oliveira, Edson Pereira Marques Filho
Validation: Maciel Piñero Sánchez
Writing – original draft: Maciel Piñero Sánchez, Amauri Pereira de Oliveira

et al., 2016; Song et al., 2005; Wang et al., 2007; Whiteman et al., 1997); Andes (Garreaud & Muñoz, 2005; Jones, 2019; Marengo et al., 2004; Montini et al., 2019); China (Du et al., 2014; He et al., 2016; Li et al., 2018; Wei et al., 2013, 2014; Zhang et al., 2019); India (Ruchith & Raj, 2015; Ruchith et al., 2014); Colima Valley, Mexico (Arfeuille et al., 2015); Cabauw, Netherlands (Baas et al., 2009); Antarctica (Andreas et al., 2000; King et al., 2008); Negev, Israel (Kutsher et al., 2012); Hannover, Germany (Emeis, 2014b); Boulogne-sur-Mer, France (Roy et al., 2021); Amazon Rain Forest (Corrêa et al., 2021; Oliveira & Fitzjarrald, 1994), Pantanal (Martins et al., 2013) and Southern Brazil (Beu, 2019; Karam, 2002).

Knowing LLJ properties is important for planning aviation safety procedures in airports (Wittich et al., 1986), assessing the potential of wind energy production (Banta et al., 2013; Emeis, 2014a), predicting transport of atmospheric pollutants, and tracking convective systems that produces heavy precipitation events (Iago et al., 2019). Some studies shows that the LLJs have an important role in the moisture transport, modulating the diurnal cycle of precipitation in eastern Andes (Jones, 2019; Marengo et al., 2004; Montini et al., 2019); Great Plains, USA (Higgins et al., 1997; Trier et al., 2014) and southwestern China (Zhang et al., 2019). Observational evidence shows that LLJ wind maximum may, through shear-sheltering mechanism, inhibit large eddies and reduce turbulent transport toward surface (Duarte et al., 2012; Martins et al., 2013; Smedman et al., 2004).

Understanding LLJs behavior is particularly important over urban areas where they can increase the vertical transport of pollutants, mainly O_3 (Banta et al., 1998; Corsmeier et al., 1997; Hu, Klein, Xue, Zhang, et al., 2013; Klein et al., 2014; Sullivan et al., 2017), which is likely due to the enhanced wind shear (Zhang et al., 2020); and interact with urban heat island (UHI) (Hu, Klein, Xue, Lundquist, et al., 2013; Kallistratova & Kouznetsov, 2012). Despite the increase in LLJs studies in recent years, due to the development of ground-based remote sensing techniques, only few have been done in urban areas, for example, in the Moscow, Russia (Kallistratova & Kouznetsov, 2012; Kallistratova et al., 2009); Oklahoma City, USA (Hu, Klein, Xue, Lundquist, et al., 2013; Wang et al., 2007); London, UK (Barlow et al., 2015) and Beijing and Guangzhou, China (Miao et al., 2018). These studies concluded that in urban areas LLJs are higher, weaker, and less frequent than in adjacent rural areas. These differences are attributed to the urban-rural contrast in roughness and surface thermal properties. There are also evidences that turbulent mixing induced by LLJ modulates UHI intensity in urban areas (Hu, Klein, Xue, Lundquist, et al., 2013).

There are few observational studies of LLJs in the metropolitan region of São Paulo (MRSP) available in the literature (Nair et al., 2004; Oliveira et al., 2020; Sánchez et al., 2020). Using a Doppler sodar, Nair et al. (2004) observed a LLJ of 21 m s^{-1} from the northeast at 1,300 m associated with the combination of thermal gradient wind and down slope mountain flow from the northern mountains of São Paulo. By analyzing the Urban Boundary Layer (UBL) diurnal evolution during a typical undisturbed day in February (summer) and August (winter) in the MRSP, Oliveira et al. (2020) found that the LLJs reached a maximum intensity (height) during the early morning in both days, varying from 4.7 m s^{-1} (357 m) in the summer to 12.8 m s^{-1} (515 m) in the winter day. Sánchez et al. (2020) developed an objective criterion to retrieve LLJ in vertical profiles of wind of rawinsonde carried during the two-field campaigns of MCITY BRAZIL Project in 2013 and concluded that the LLJs appear in 80% of the days in the MRSP. These LLJs occurred between 95 and 962 m, with speed varying from 2.7 to 14 m s^{-1} and blowing predominantly from north-east quadrant.

One goal of this work is to expand the investigation of Sánchez et al. (2020) by developing and applying a new algorithm to retrieve the main features of the LLJs observed in the MRSP, such as frequency of occurrence, height (Z_{LLJ}), intensity (V_{LLJ}) and direction (D_{LLJ}), using rawinsonde carried regularly twice a day during four years from 2009 to 2013. Another goal is to deepen the previously investigation of Sánchez et al. (2020) using rawinsondes carried out every 3-hr during the two 10-day field campaigns of the MCITY BRAZIL Project in February and August of 2013. Although, Sánchez et al. (2020) is the most detailed description of LLJs in the MRSP available so far, they did not address the impact of synoptic and mesoscale systems on the LLJs, the role of inertial oscillation in their formation and their relationship with other urban climate features of the MRSP, such as UHI intensity, SIL strength, concentration of particulate matter 2.5 ($PM_{2.5}$) and carbon monoxide (CO) at the surface. Both rawinsondes data set used in this investigation were performed in the "*Campo de Marte*" Airport (ACM), north of São Paulo City (Figure 1).

The region of study and climate are presented in Section 2. Measurements and methods used to estimate the LLJ properties are described in Sections 3 and 4. The LLJ properties are presented and discussed in Section 5. The conclusions are summarized in Section 6.

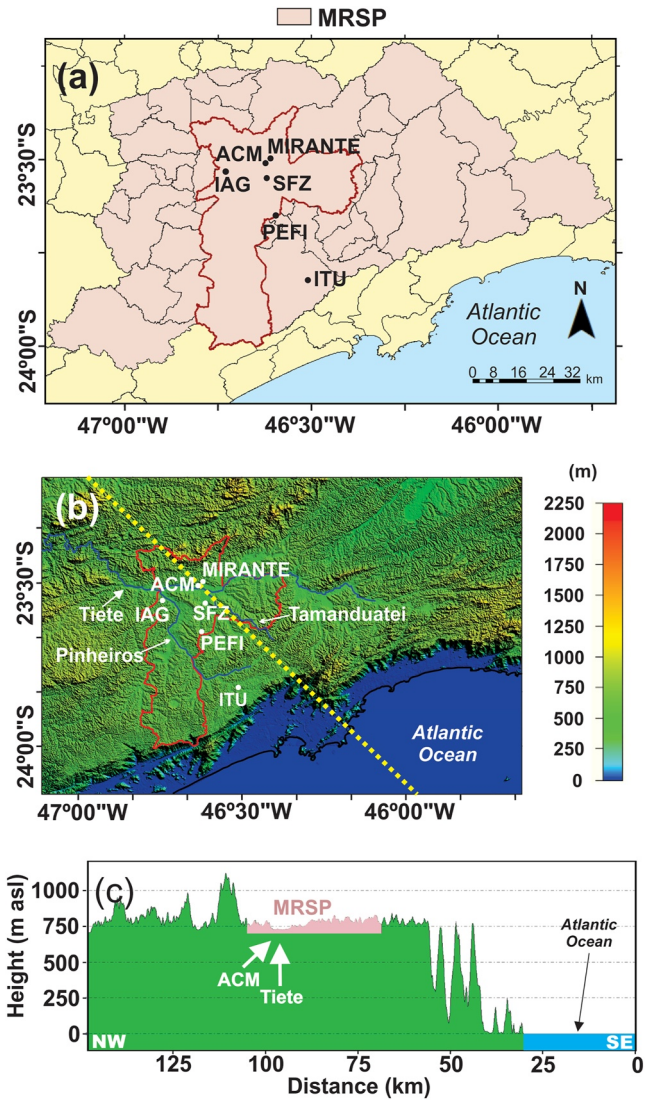

Figure 1. Geographic features of the metropolitan region of São Paulo (MRSP). In (a) the city of São Paulo (23°33′1″S; 46°38′2″W; 760 m asl) is indicated by red and the remaining 38 cities by black borders. The rawinsonde site is indicated by "*Campo de Marte*" Airport (ACM) and meteorological sites by SFZ, ITU, IAG, PEFI and MIRANTE. The dotted yellow line in (b) indicates a 150-km cross section perpendicular to the coastline, oriented in the northwest to southeast direction and passing by ACM. Topography and MRSP limits along of this cross section are shown in (c). Topography is based on the highest-resolution topographic data (3-arc-second Resolution—90 m) generated from NASA's Shuttle Radar Topography Mission, available at https://www2.jpl.nasa.gov/srtm/.

2. Region of Study and Climate

The MRSP is in the southeastern Brazil on the "*Paulista*" plateau at 722 m above sea level (asl) and 65 km from the Atlantic Ocean. It is a conurbation of 39 municipalities (Figure 1a), where live 21.7 million habitants (IBGE, 2019). The topography of the MRSP is complex (Figures 1b and 1c), with the urban area located on the plateau bounded in the north and northwest by a chain of hills ranging from 300 to 700 m and, in the southeast by the "*Serra do Mar*" slopes. The topography of the urban area is composed by three river valleys: "*Tiete*" (east-west oriented), "*Tamanduatei*" and "*Pinheiros*" (northwest-southeast oriented).

The climate characterization of the MRSP is based on monthly mean values obtained between 1960 and 1990 on the meteorological surface station of MIRANTE (23°29′47″S; 46°37′11″W; 792 m asl). According the Köppen classification of Alvares et al. (2014), the climate of MRSP is classified as high elevation subtropical humid (Cwb), with dry and mildly cold winters (June-August), and wet and warm summers (December–February). The minima air temperature (15.8°C) and specific humidity (9.1 g kg^{-1}) occur in July, and precipitation (39.6 mm) in August. The maxima air temperature (22.4°C) and specific humidity (14.6 g kg^{-1}) occur in February, and precipitation (237 mm) in January (Oliveira et al., 2003; Sánchez et al., 2020).

Large-scale air circulation in the MRSP is controlled by the semi-permanent South Atlantic Subtropical High (SASH) and continental low-pressure systems, which induce weak surface winds from north-northeast sector during summer and from northeast-east sector in winter (Oliveira et al., 2003). The minimum wind intensity (2.3 m s^{-1}) occurs in May and the maximum (3.1 m s^{-1}) in November (Sánchez et al., 2020). The large-scale pattern is often disturbed by the passage of CF throughout the year, which induces pre-frontal northwest winds and post-frontal southeast winds.

Based on four years of rawinsondes carried out daily at 2100 LT from September 2009 to August 2013 in the ACM, Sánchez et al. (2020) concluded that the largest UBL height occurs in May (1,632 ± 96 m) and the minimum in September (1,061 ± 77 m). This pattern responds to the seasonal variation in the cloudiness pattern associated to disturbances caused by synoptic and mesoscale systems in the MRSP.

In addition to these large and synoptic scales systems, the MRSP is influenced by the following meso and local-scale circulations: Sea Breeze (SB), mountain-valley and UHI centripetal circulations (Ribeiro et al., 2018). These thermally induced circulations rise from horizontal thermal contrasts induced by land-ocean thermal capacity differences, topography, and land use configuration of the MRSP (Figure 1c). The SB penetrates inland into the MRSP plateau early in the afternoon in more than 50% of the days, with higher frequency during summer and winter-to-summer transition (August–November). The passage of SB front is preceded by northwest winds that shifts to southeast (Oliveira et al., 2003). According to Ribeiro et al. (2018), advection of cold and wet maritime air associated with the SB disrupts the UBL growth and induces the formation of a thermally stable internal boundary layer. There are also evidences that UHI and SB circulation under appropriated upper air synoptic conditions can produce severe weather over MRSP (Vemado & Pereira Filho, 2016).

3. Measurements and Data

3.1. Soundings

This work is based on two sets of rawinsondes carried out at the ACM (23°30′32" S; 46°38′04″W; 722 m asl, Figure 1):

1. 160 soundings released with a frequency of one in every three hours during two periods of 10 consecutive days, in the summer (19–28 February, 2013) and winter (6–15 August, 2013) MCITY BRAZIL Project campaigns (Oliveira et al., 2020).
2. 2611 soundings carried out regularly twice a day at 0900 LT (1200 GMT) and 2100 LT (0000 GMT) from 1 September 2009, to 15 August 2013.

Soundings are performed by a DIGORA III data acquisition system and radiosonde model RS92-GSP, both manufactured by Vaisala, Inc. A description of the equipment characteristics and measurements accuracy can be found in Sánchez et al. (2020). The vertical resolution of rawinsondes in the first 4,000 m, given by the mean vertical distance between two consecutive points from surface to 4,000 m, is 62 and 302 m for fine (MCITY) and coarse (Regular) resolution soundings, respectively. The impact of vertical resolution on the LLJs identification is analyzed in Section 4.

3.2. UHI Intensity

UHI intensity (ΔT) is estimated in the MRSP from near-surface (pedestrian level) air temperature differences between urban (T_{urban}) and rural (T_{rural}) sites, respectively, SFZ and ITU, as: $\Delta T = T_{\text{urban}} - T_{\text{rural}}$. The site SFZ (23°33′01″S; 46°37′49″W; 741 m asl) comprises a 10-m tower set up in the center of a metallic platform on the top of an 18-story building, 77 m above ground level (agl) in the São Paulo City downtown area (Figure 1a). The site ITU (23°49′32″S; 46°30′32″W; 760 m asl) consists of a 10-m tower set up at the surface level in a vegetated area in "*Itutinga Pilões*" State Park located at south of the MRSP (Figure 1a). They are performed by air temperature sensors model CS215, manufactured by Campbell Sci Inc, USA, set up at 78.6 m agl (SFZ) and 1.6 m agl (ITU). A complete description of the quality control procedures applied to temperature measurements at SFZ and ITU sites is described in Oliveira et al. (2020).

In these two sites, continuous and simultaneous observations of air temperature are carried out with sample frequency of 0.5 Hz and stored as 5-min average since 4 July 2013. Therefore, the UHI intensity can only be estimated using in situ observation at SFZ and ITU sites during the field campaign carried out in the winter of 2013 (6–15 August). Besides, measurements of the surface temperature in the SFZ site started only in December 2016. To estimate surface temperature at SFZ site during the winter field campaign of August of 2013, the hourly values of temperature measured at the top of the building (78.6 m agl) are extrapolated to the surface (1.5 m agl). The extrapolation is based on an empirical expression $T_{\text{urban}} = T_{1.5} = 1.868 + 1.004 * T_{78.6}$, obtained by fitting a first order polynomial through the dispersion diagram of the temperature measured in the surface at 1.5 m agl ($T_{1.5}$) versus temperature measured in the top of the building at 78.6 m agl ($T_{78.6}$), simultaneously during all months of August from 2017 to 2019. This dispersion diagram (not show here) showed that hourly values of $T_{78.6}$ and $T_{1.5}$ have a linear distribution with a Pearson's coefficient of 0.99. Similar procedure has been used for developing empirical expressions to diagnosticate hourly values of diffuse and other components of solar radiation at the surface (Furlan et al., 2012; González-Rodríguez et al., 2021).

3.3. Geostrophic Wind

The geostrophic wind is evaluated from the geopotential height obtained every three hours at pressure levels of 925, 900, 875, 850, 825 and 800 hPa from ERA5 reanalysis data set (https://cds.climate.copernicus.eu/cdsapp%23%21/dataset/reanalysis%2Dera5%2Dpressure%2Dlevels%3Ftab%3D%20form) produced by the European Center for Medium-Range Weather Forecasts (ECMWF). Zonal (u) and meridional (v) wind components are also obtained from the ERA5 reanalysis, with same spatial and temporal resolution. In both cases horizontal domain corresponds to 18–28°S and 41–51°W, with a horizontal resolution of 0.25° by 0.25°. In the geostrophic and actual winds obtained from reanalysis described here are used as reference to identify when LLJs observed in the MRSP are sub or super geostrophic and to clarify the inertial oscillation mechanism.

3.4. Particulate Matter 2.5 and Carbon Monoxide

Particulate matter 2.5 and carbon monoxide concentrations measured at the surface during winter field campaign of 2013 (6–15 August) are used in Section 5.4. These measurements were carried out in the air quality monitoring network station of the State São Paulo Environmental Company (*"Companhia Ambiental do Estado de São Paulo"*, CETESB). This station is in the São Paulo City urban area (23°33′39″S; 46°42′06″W; 721 m asl) characterized by an intense vehicle traffic. Located at 4 km east of IAG and close to *"Pinheiros"* river (Figure 1b), this stations yielded hourly values of $PM_{2.5}$ (μg m^{-3}) and CO (ppm), sampled by an infra-red absorption monitor, model 48i, and a beta-continuous ambient particulate monitor, model 5014i, both manufactured by Thermo Scientific™ Electron Corporation, USA. Calibration and quality control procedures applied to these measurements are described in Dominutti et al. (2016).

4. Methodology

A variety of LLJ identification criteria based on vertical horizontal-wind profiles can be found in the literature. Some authors consider a LLJ when a local maximum exceeds the wind speed above and below by a threshold of 1 m s^{-1} (Kallistratova et al., 2009; Kallistratova & Kouznetsov, 2012). Others use a threshold of 2 m s^{-1} (Andreas et al., 2000; Karipot et al., 2009). Banta et al. (2002) tested threshold values and found a critical value of 0.5 m s^{-1}. Some authors categorize LLJs in terms of intensity by considering ranges of local maximum wind speed between 5 and 20 m s^{-1} and threshold between 2 and 10 m s^{-1} (Arfeuille et al., 2015; Bonner, 1968; Miao et al., 2018; Song et al., 2005; Wei et al., 2013, 2014; Whiteman et al., 1997). According to Kallistratova and Kouznetsov (2012) threshold values, and as consequence the identification of LLJ, are sensitive to the vertical resolution of the wind speed measurements.

4.1. LLJ Identification Criteria

As indicated in the survey above, most of criteria to identify LLJs are tailored considering local climate conditions and measurements resolution. According to Sánchez et al. (2020), in the case of the MRSP it is more convenient to use a criteria based on Baas et al. (2009), which defines the LLJ as the lowest wind speed maximum in the first 500 m that is: 2 m s^{-1} and 25% faster than the next minimum. These criteria were used to identify LLJ in Cabauw, Netherlands, from observations made with wind profiler/radio acoustic sounding systems. Taking into account that LLJs in urban regions are higher and weaker than in rural regions (Kallistratova & Kouznetsov, 2012; Kallistratova et al., 2009), rural LLJ criteria proposed by Bass et al. (2009) was adapted for urban area of the MRSP by considering the following changes:

1. Maximum wind speed at the jet nose in the lowest 1,000 m is greater or equal to 2.0 m s^{-1} and 25% faster than next minimum.
2. It is only considered a LLJ event when this local maximum is observed in at least two consecutive soundings (persistence criterion).

Thus, the LLJ definition proposed by Baas et al. (2009) was extended to 1,000 m and the threshold difference between maximum and minimum of 2 m s^{-1} was replaced by a single lower limit of 2 m s^{-1} to prevent small oscillations in the wind speed profile being considered as LLJ. Examples of LLJs that satisfy all criteria described above are indicated in Figure 2a for two consecutive soundings carried out during the field campaigns (MCITY) and in Figure 2b for one regular sounding (Regular). The persistence criterion holds only for MCITY soundings because they are performed every 3 hours (Figure 2a). In this case, a LLJ event is defined as sequence of soundings in which LLJs are detected in at least two consecutive soundings. In the case of regular soundings, where the interval between soundings is 12 hr at least, the LLJ event was defined when: (a) it is detected simultaneously at 2100 LT and at 0900 LT of the next day; (b) it is detected at 2100 LT and it is not detected at 0900 LT of the next day; (c) it is detected at 0900 LT and it is not detected at 2100 LT of the night before. According to this classification it is possible to have two LLJ events during one unique day.

Since it is not possible to apply these criteria in the visual examination of a large data set, such as in the case of 2,611 regular soundings, an algorithm was developed to identify LLJ structures. Therefore, in this study the main properties of the LLJs are estimated using vertical profile of wind speed and direction retrieved from rawinsondes carried out every three hours during 10-day field campaigns of February and August in 2013 (hereafter indicated

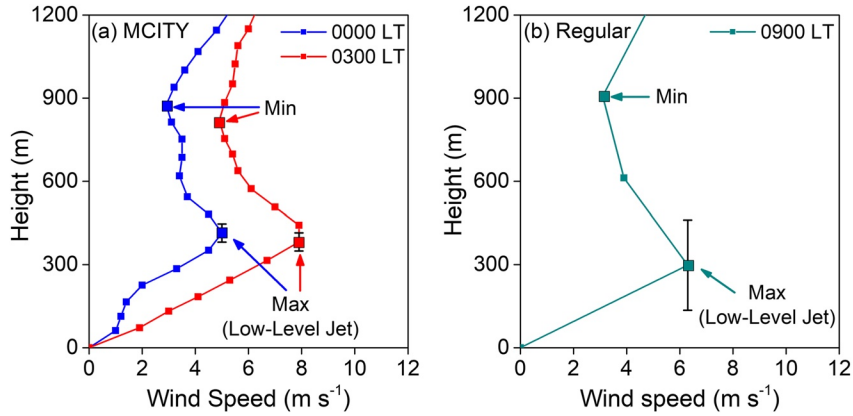

Figure 2. Examples of low-level jet structure that satisfy the objective criteria for soundings carried out during (a) 10 August 2013, at 0000 LT and 0300 LT (MCITY-sounding) and (b) 24 July 2012, at 0900 LT (Regular-sounding). Vertical bars indicate uncertainty due to the resolution of 62 m (MCITY) and 302 m (Regular).

by MCITY or MCITY-soundings) and regularly twice a day from 1 September 2009, to 16 August 2013 (hereafter indicated by Regular or regular-soundings).

Considering the inherent variability presented by the vertical wind structure in the lower atmosphere that often displays multiple maxima, it is plausible to assume that visual inspection allows one to identify the LLJ structure with greater accuracy compared to the automatic algorithm (Banta et al., 2002; Kallistratova et al., 2009). Kallistratova et al. (2009) used an automatic method based on cluster analysis and were able to recognize only 20% of the visually identified LLJs. Another algorithm, used by Banta et al. (2002) to identify LLJ over southeast Kansas, excluded also many visually identified LLJs.

The algorithm developed in the present study was able to capture 89% and 96% of the LLJs using, respectively, fine and coarse resolution soundings. These surprisingly high percentages are intrinsically related to the criteria adopted here and the resolution of the soundings.

According to the criteria adopted in this work, LLJ event occurs when the difference between the maximum (below 1,000 m) and the next minimum wind speed above is larger than 25%. This criterion differs from others available in the literature. For instance, Banta et al. (2002) defined a LLJ event when a low-level wind speed maximum exhibits a decrease of at least 2 m s^{-1} in the next level above and below the level of the peak value. Kallistratova et al. (2009) defined LLJ event when local maximum exceeds by 1 m s^{-1} the wind speeds above and below. Comparatively to the criterion used in our work, these criteria are very restrictive because they use points immediately adjacent to the maximum wind speed point. In our case, the minimum may occur in points far from the wind speed maximum point. This explains why our algorithm has a much larger rate of success (89% and 96%) in comparison to 20% of Kallistratova et al. (2009). Vertical resolution of wind speed profiles does also contribute to the success of detection algorithm developed in this work. Any threshold of wind vertical variation is more difficult to satisfy when vertical distance between two consecutive points is small. Banta et al. (2002), used data collected by Doppler lidar with a vertical resolution of 30 m, while Kallistratova et al. (2009) used data collected by Doppler sodar with a vertical resolution of 20 m. In our case, the vertical resolution of fine-resolution soundings is 62 m and coarse-resolution is 302 m. The chance to satisfy our criteria is much higher than the other criteria. In vertical wind profiles with coarser resolution small scale oscillations are filtered out reducing the main cause misidentification. Therefore, the algorithm performance for fine resolution soundings is good (89%) but, is not as good as for coarse resolution (96%), due to the combination of all these factors. The performance of the algorithm is analyzed in more detailed in the next section.

4.2. Validation of Detection Algorithm

The detection algorithm was validated by comparing its capability to identify LLJ properties (Z_{LLJ}, V_{LLJ} and D_{LLJ}) with the visual inspection using two different resolution data sets: 80 fine-resolution soundings (~62 m) carried out during field campaigns of February and August of 2013 (Figures 3a, 3c and 3e) and 85 coarse-resolution

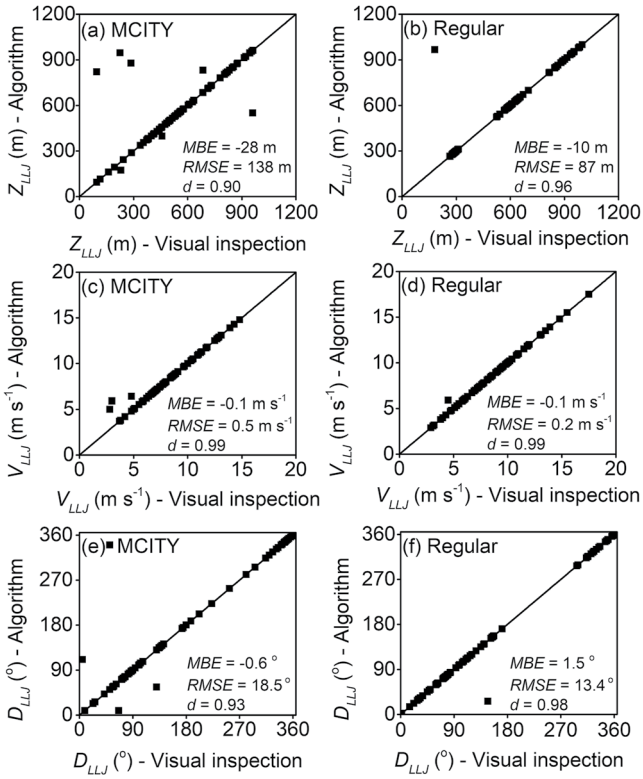

Figure 3. Dispersion diagrams of low-level jet height, intensity and direction estimated by visual inspection and algorithm of rawinsondes carried out, respectively, during (a), (c), (e) both MCITY field campaigns in 2013 (MCITY), and (b), (d), (f) regularly (Regular) from June to August of 2012.

soundings (~302 m) carried out during June and August of 2012 (Figures 3b, 3d and 3f). The comparison is made using three statistical parameters: Mean Bias Error (*MBE*), Root Mean Square Error (*RMSE*) and Index of Agreement (*d*). The best combination of these metrics are small absolute values of *MBE* and *RMSE*, and *d* close to 1. In this case, negative *MBE* indicates that LLJ properties retrieved by algorithm overestimate the ones by visual inspection. In general, the algorithm has an excellent performance for all LLJ properties regardless of the sounding resolution. There is a noticeable better agreement between visual inspection and detection algorithm using coarse resolution soundings to estimate Z_{LLJ} and D_{LLJ}. For Z_{LLJ}, the *MBE*, *RMSE*, and *d* are, respectively, −28 m (−10 m), 138 m (87 m) and 0.90 (0.96) for MCITY (regular) soundings. For D_{LLJ}, the *MBE*, *RMSE* and *d* are −0.6° (1.5°), 18.5° (13.4°) and 0.93 (0.98) for MCITY (regular) soundings. On the other hand, for V_{LLJ} the agreement is equally excellent for MCITY and regular soundings. These results indicate that the proposed algorithm can be used with good accuracy to identify LLJ properties such as Z_{LLJ}, V_{LLJ} and D_{LLJ}, regardless the vertical resolution of the soundings.

To illustrate the impact of sounding vertical resolution, Z_{LLJ}, V_{LLJ} and D_{LLJ} are estimated by applying the detection algorithm in simultaneous fine (MCITY) and coarse-resolution (Regular) soundings carried out during the field campaigns of 2013 (Figure 4). This comparison was possible because coarse-resolution soundings were also available during the field campaigns. An excellent agreement was observed between the algorithm performance using coarse and fine resolution (Figures 4a–4c).

Using MCITY soundings as reference, the algorithm yield Z_{LLJ}, V_{LLJ} and D_{LLJ}, respectively, with *MBE* equal to −33 m, 0.5 m s^{-1}, and 3°, *RMSE* equal to 88 m, 0.7 m s^{-1}, and 5.4°, and with *d* equal to 0.95, 0.97 and 0.99, respectively. These results show that the LLJ properties are only slightly sensitive to rawinsonde resolution. In general, applying the algorithm to coarse resolution soundings overestimate Z_{LLJ} (*MBE* < 0) and underestimate V_{LLJ} and D_{LLJ} (*MBE* > 0) with respect to the fine resolution soundings. The excellent agreement can be verified in the soundings of 0900 LT on 28 February 2013 (Figures 4d and 4e) and 0900 LT on 7 August 2013 (Figures 4f and 4g). In the first case, Z_{LLJ}, V_{LLJ} and D_{LLJ} obtained with fine and coarse vertical resolution coincide (Figures 4d and 4e). In the second case, Z_{LLJ} and V_{LLJ}, estimated with coarse resolution are, respectively, 139 and 0.8 m s^{-1} lower than fine resolution, while both D_{LLJ} are similar.

4.3. Impact of Resolution on the LLJ Properties

Even though the analyses in the previous subsections indicate that the algorithm developed in this study performs quite satisfactorily to retrieve LLJ events, using fine or coarse resolution sounding, they also indicated that sounding resolution affect the accuracy of LLJ properties.

The biggest impact of the sounding resolution is on the Z_{LLJ}. In the case of MCITY fine resolution soundings, the uncertainty of Z_{LLJ} is equal to 62 m, the average sounding resolution. Similarly, in the case of regular soundings, uncertainty of Z_{LLJ} is equal to 302 m. Therefore, the accuracy for Z_{LLJ} is equal to ±151 m for regular (coarse resolution) and ±31 m MCITY (fine resolution) soundings (Figure 2).

On the other hand, the impact of sounding resolution on the accuracy of the other properties such as V_{LLJ} and D_{LLJ} depend on the specific features of the LLJ.

Intuitively, if the LLJ has a vertical extension wider than the sounding-resolution range, the algorithm yields quite accurate values of V_{LLJ}. Indeed, the LLJs observed during the field campaigns in 2013 have a mean width of 816.9 ± 36 m, what is considerably larger than the 302-m sounding resolution range. The impact of sounding resolution on LLJ intensity was analyzed (not shown here) considering the difference between the theoretical intensity of an idealized LLJ (Gaussian-symmetric shape) and intensity retrieved by the algorithm considering

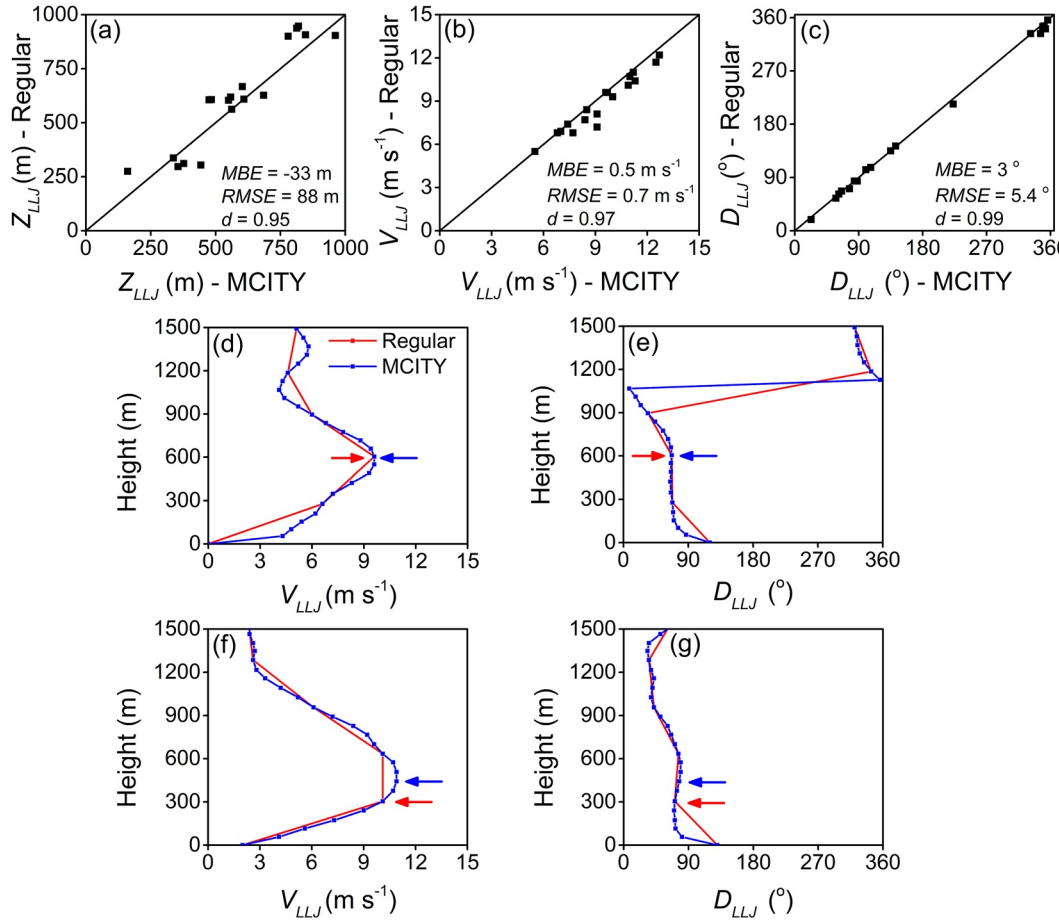

Figure 4. Dispersion diagrams of low-level jet (LLJ) (a) height, (b) intensity and (c) direction estimated by the algorithm. Vertical profiles of (d) wind speed and (e) direction on 28 February 2013, at 0900 LT. Vertical profiles of (f) wind speed and (g) direction on 7 August 2013, at 0900 LT. Fine and coarse resolution soundings are indicated by blue and red, respectively. The arrows in (d)–(g) indicate the LLJ heights.

the representation of idealized LLJ in the vertical grid with grid size equal to 300 m and equivalent to resolution of coarse sounding of 302 m. For LLJ widths varying from 200 to 800 m, the difference between theoretical (Gaussian-shape LLJ) and retrieved intensity of LLJ speed is less than 0.2 m s^{-1} for most of the cases. Therefore, in this specific case it will be assumed that sounding resolution has a minimal impact on the V_{LLJ}, and the uncertainty is set equal to the wind speed measurement error of 1 m s^{-1} (Sánchez et al., 2020).

Similarly, the impact of sounding resolution on the accuracy of D_{LLJ} depend on the intensity of the LLJ directional shear. Observations during the field campaigns of 2013 indicate that the LLJs with mean width of 816.9 ± 36 m display a mean wind direction shear of 40 ± 3°. Therefore, it seems plausible to assume that the impact of vertical resolution results in an uncertainty of ±20° in the D_{LLJ}.

5. Results and Discussions

5.1. Synoptic and Mesoscale Effects

The impact of synoptic and mesoscale systems on the diurnal evolution of the wind speed in the first 1,500 m in the MRSP during both field campaigns of 2013 is shown in Figure 5. In general, LLJs take place at nights when sky is clear or partially cloudy and light surface winds prevails. These conditions are most often observed under synoptic systems that induce subsidence and anticyclonic circulation in the MRSP, such as Upper Tropospheric Cyclonic Vortex (UTCV), SASH and post-frontal High Pressure System (HPS). These synoptic systems prevailed, during eight LLJ events on the nights of February (19–20, 20–21, 21–22, 23–24, 24–25, 25–26, 27–28,

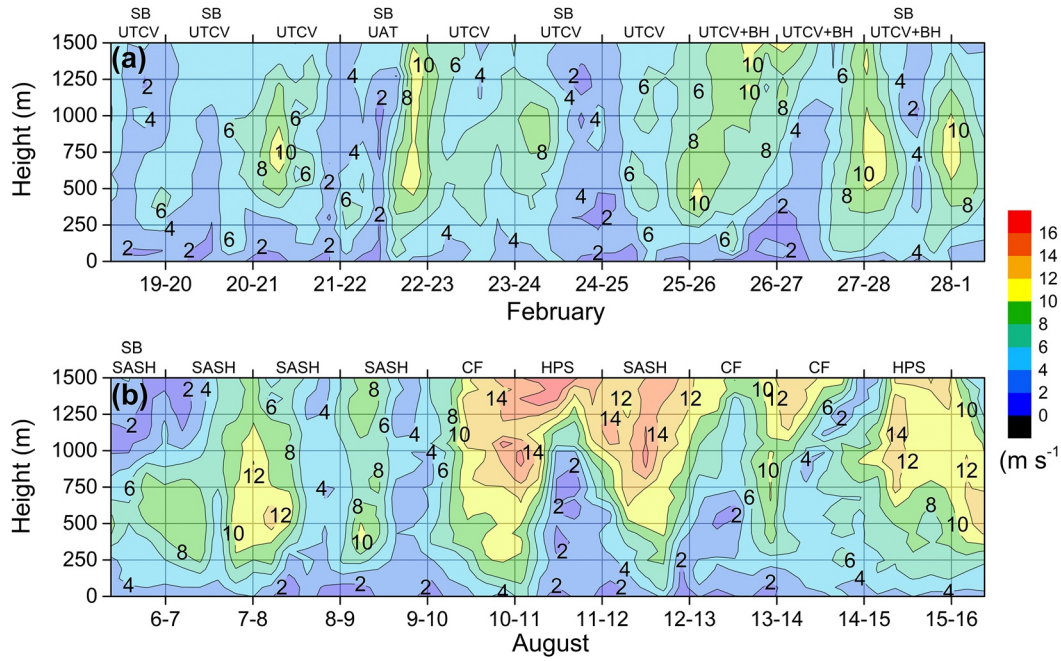

Figure 5. Time evolution of the wind speed (m s^{-1}) in the metropolitan region of São Paulo during (a) summer, and (b) winter field campaigns of the MCITY BRAZIL Project in 2013. Symbols at the top correspond to: UTCV = Upper Tropospheric Cyclonic Vortex; SB = Sea Breeze; UAT = Upper Air Trough; BH = Bolivia High; HPS = post-frontal High Pressure System; SASH = South Atlantic Subtropical High; CF = Cold Front (Sánchez et al., 2020).

28–1, Figure 5a) and seven on the nights of August (6–7, 7–8, 8–9, 9–10, 11–12, 12–13, 15–16, Figure 5b) field campaigns, as it will be described in the next subsections. In these analyses sky cover observation between 0700 and 2400 LT in the PEFI surface station is used to characterize the cloudiness in the MRSP (Tables 1 and 2). The high correlation ($r = -0.80$) between the net radiation (assumed by convention negative when downward into the surface and vice versa) measured at the IAG and sunshine duration measured at the PEFI station, indicates that PEFI observation of cloud can be assumed as representative of the MRSP. A more complete description of the main synoptic systems that were affecting the weather in the MRSP during field campaigns of 2013 can be found in Sánchez et al. (2020).

5.1.1. Summer Campaign

5.1.1.1. Synoptic Scale Systems

Although favorable synoptic scale conditions prevailed on seven out of 10 nights, nine LLJ events were detected during summer field campaign (Figure 5a). The clear-sky (three) and partially cloudy (four) conditions were observed during seven nights on 19–20, 20–21, 21–22, 24–25, 25–26, 27–28 February, and 28-March 1 and are associated to subsidence induced by a semi stationary UTCV positioned northeast of the MRSP. In these cases, the mean values of nighttime sky cover and net radiation were, respectively, 5 ± 1 okta and 47.6 ± 4 W m^{-2} (Table 1). Except for the night of 24–25 February, these LLJ events presented maximum intensity between 0000 and 0600 LT, ranging from 7.7 to 13.1 m s^{-1}, from the northwest and northeast quadrants and between 372 and 831 m. These LLJs started between 1800 and 0000 LT and lasted between 6 and 21 hr. The event on the night of 24–25 February differs from the typical summer events described above because its maximum intensity (8.0 m s^{-1}) occurred at 1500 LT, blowing from northwest at 383 m (Table 1). There is no clear reason for this middle of afternoon maximum.

Despite the UTCV, the presence of cloud during the LLJ events on the night of 27–28 February and 28-March 1 are due to a high-level horizontal divergence induced by the interaction between Bolivia High (BH) and UTCV circulations. The BH circulation was particularly strong on 26 February producing 39.0 mm of rain in the MRSP, and no LLJ event was observed in the nighttime of 26–27 February. However, this disturbance that favored clouds on 26–27 February subsided progressively and LLJ events were observed during nighttime of 27–28 February and 28 February–1 March.

Earth and Space Science
10.1029/2021EA002190

Table 1
Synoptic and Mesoscale Systems Acting in the MRSP During Summer (19–28 February 2013) Field Campaign of the MCITY BRAZIL Project

Field campaign	Night	LLJ Onset (LT) and duration (hrs.)	LLJ Maximum Time (LT)	LLJ Maximum Z_{LLJ} (m)	LLJ Maximum V_{LLJ} (m s^{-1})	LLJ Maximum D_{LLJ} (°)	Prevailing meteorological conditions	Prevailing synoptic system	Day	SB onset (LT)	Rain (mm)	Sunshine duration (hrs.)	Sky cover[a] (okta) Daytime	Sky cover[a] (okta) Nighttime	Net radiation[b] (W m^{-2}) Daytime	Net radiation[b] (W m^{-2}) Nighttime	Horizontal wind speed (m s^{-1}) and direction (°) Daytime	Horizontal wind speed (m s^{-1}) and direction (°) Nighttime
Summer (February)	19–20	2100 9	0000	379	7.7	42	Partially cloudy and light wind	UTCV	19	1200	1.4	6.7	5	6	−289	42[c]	1.4 ± 0.2 123 ± 27	1.1 ± 0.2 57 ± 10
	20–21	2100 12	0600	728	13.1	360	Clear sky and light wind	UTCV	20	1400	0	10.1	1	1	−453[c]	58[c]	1.7 ± 0.1 70 ± 13	0.6 ± 0.1 131 ± 8
	21–22	0000 6	0300	372	8.6	281	Clear sky and light wind	UTCV	21	–	0	11.2	2	3	−464[c]	61[c]	2.4 ± 0.3 315 ± 18	1.0 ± 0.2 274 ± 20
	22–23	1500 3	1800	624	13.1	173	Cloudy and light wind	UAT	22	1200	23.7	6.7	4	8	−281	15	1.8 ± 0.2 195 ± 18	1.2 ± 0.1 144 ± 6
	23–24	1800 21	0600	922	10.4	56	Cloudy and light wind	UTCV	23	–	4.6	0.8	8	8	−210	22	1.7 ± 0.2 165 ± 4	0.8 ± 0.1 117 ± 5
	24–25	2100 18	1500	383	8.0	314	Partially cloudy[d] and light wind	UTCV	24	1300	14.7	8.8	7	8	−383[c]	35	1.9 ± 0.1 76 ± 14	0.7 ± 0.1 228 ± 22
	25–26	1800 6	0000	410	12.8	326	Clear sky[d] and light wind	UTCV	25	–	0.1	9.1	3	7	−377[c]	52[c]	2.5 ± 0.2 313 ± 7	1.6 ± 0.2 305 ± 4
	26–27	–	–	–	–	–	Cloudy and light wind	UTCV + BH	26	–	39.0	7.2	4	8	−352	26	2.6 ± 0.3 302 ± 14	0.7 ± 0.2 158 ± 0.1
	27–28	1800 21	0600	804	11.0	72	Partially cloudy and light wind	UTCV + BH	27	–	0.1	2.9	7	6	−355[c]	37	1.6 ± 0.2 158 ± 6	1.5 ± 0.1 90 ± 6
	28–01	1800 15	0300	831	11.7	90	Partially cloudy and light wind	UTCV + BH	28	1400	0	4.9	6	4	−330	48[c]	2.0 ± 0.2 98 ± 11	2.2 ± 0.2 82 ± 8

[a]Daytime = 0700–1800 LT and nighttime = 1800–2400 LT. [b]Daytime = 0600–1800 LT and nighttime = 1800–0600 LT. Rain, sunshine duration, sky cover and wind speed and direction were measured at PEFI climatological station. Net radiation was measured in the IAG (Oliveira et al., 2020). [c]Day and night values higher than mean values observed during field campaign of August (−353 W m^{-2}, 41 W m^{-2}) in the IAG. Incoming downward and outgoing upward net radiations at the surface are, respectively, negative and positive. [d]High clouds.

Earth and Space Science
10.1029/2021EA002190

Table 2
Synoptic and Mesoscale Systems Acting in the MRSP During Winter (6–15 August 2013) Field Campaign of the MCITY BRAZIL Project

Field campaign	Night	LLJ: Onset (LT) and duration (hrs.)	LLJ: Maximum Time (LT)	LLJ: Maximum Z_{LLJ} (m)	LLJ: Maximum V_{LLJ} (m s^{-1})	LLJ: Maximum D_{LLJ} (°)	Prevailing meteorological conditions	Prevailing synoptic system	Day	SB onset (LT)	Rain (mm)	Sunshine duration (hrs.)	Sky cover[a] (okta) Daytime	Sky cover[a] (okta) Nighttime	Net radiation[b] (W m^{-2}) Daytime	Net radiation[b] (W m^{-2}) Nighttime	Horizontal wind speed (m s^{-1}) and direction (°) Daytime	Horizontal wind speed (m s^{-1}) and direction (°) Nighttime
Winter (August)	06–07	1800 18	0900	450	10.9	77	Clear sky and light wind	SAHS	06	1100	0	5.6	4	0	−303[c]	60[c]	1.9 ± 0.2 118 ± 21	0.4 ± 0.0 106 ± 4
	07–08	1800 15	0600	515	12.8	9	Clear sky and light wind	SAHS	07	–	0	8.1	3	0	−331[c]	69[c]	2.5 ± 0.2 59 ± 3	2.3 ± 0.2 36 ± 6
	08–09	0000 12	0600	414	11.0	358	Partially cloudy[d] and light wind	SAHS	08	–	0	8.5	3	6	−323[c]	60[c]	2.1 ± 0.2 343 ± 10	0.4 ± 0.1 315 ± 0.0
	09–10	2100 12	0900	780	11.2	332	Partially cloudy[d] and light wind	SAHS	09	–	0	7.4	7	3	−305[c]	65[c]	1.8 ± 0.2 337 ± 10	0.8 ± 0.1 16 ± 12
	10–11	–	–	–	–	–	Cloudy and strong wind	CF	10	–	0	8.5	2	2	−328[c]	62[c]	2.9 ± 0.4 339 ± 10	3.7 ± 0.1 295 ± 2
	11–12	0300 6	0900	733	14.8	320	Partially cloudy and light wind	HPS	11	–	0	5.3	8	5	−251	67[c]	1.7 ± 0.1 235 ± 19	0.7 ± 0.1 109 ± 7
	12–13	0300 9	0300	156	5.8	66	Clear sky and light wind	SASH	12	–	0	7.8	0	0	−357[c]	63[c]	2.9 ± 0.4 327 ± 15	0.7 ± 0.1 326 ± 22
	13–14	–	–	–	–	–	Cloudy and light wind	CF	13	–	0	4.9	7	5	−234	53	1.8 ± 0.2 30 ± 6	1.7 ± 0.1 130 ± 22
	14–15	2100 9	0600	955	14.3	180	Cloudy and light wind	CF	14	–	3.4	0	8	8	–	30	2.4 ± 0.2 176 ± 3	2.1 ± 0.1 176 ± 3
	15–16	0300 6	0900	545	13.9	76	Cloudy and light wind	HPS	15	–	3.6	0.4	8	8	−201	30	1.9 ± 0.1 158 ± 0.0	1.3 ± 0.1 131 ± 9

[a]Daytime = 0700–1800 LT and nighttime = 1800–2400 LT. [b]Daytime = 0600–1800 LT and nighttime = 1800–0600 LT. Rain, sunshine duration, sky cover and wind speed and direction were measured at PEFI climatological station. Net radiation was measured in the IAG (Oliveira et al., 2020). [c]Day and night values higher than mean values observed during field campaign of August (−268 W m^{-2}, 55 W m^{-2}) in the IAG. Incoming downward and outgoing upward net radiations at the surface are, respectively, negative and positive. [d]High clouds.

Differently from typical summer events, cloudy conditions predominated during the night of 22–23 February and no LLJ event was observed. However, according to the criteria described in Section 4.1, a LLJ event was observed during daytime in the 22 February, that started as 1500 LT and lasted for 3 hr (Table 1). This event occurred under disturbed synoptic conditions caused by the passage of a shortwave Upper Air Trough (UAT). This LLJ event is more likely associated with the SB front passage through the MRSP. During daytime period of 22 February, sunshine duration, sky cover and net radiation were, respectively, 6.7 hr, 4 okta and -281 W m^{-2} (Table 1). It reached maximum intensity of 13.1 m s^{-1} at 1800 LT, blowing from south at 624 m (Table 1). After 1800 LT, the atmospheric conditions in the MRSP becomes very unstable due to the combination of SB and shortwave UAT, producing 23.7 mm of rain and inhibiting the overnight LLJ development.

Even though the LLJ event in the night of 23–24 February occurred under synoptic conditions associated to UTCV, it differs from the typical summer events because it occurred under cloudy conditions resulting from the passage of a UAT during previous day. The nighttime sky cover and net radiation were, respectively, 8 okta and 22 W m^{-2} (Table 1). It displayed a maximum intensity of 10.4 m s^{-1} at 0600 LT, blowing from northeast at 922 m. This LLJs started as 1800 LT and lasted for 21 hr (Table 1).

5.1.1.2. Mesoscale System

In the summer, synoptic conditions favoring LLJ events also fomented SB circulation in the MRSP. For instance, on 19, 20, 22, 24, and 28 February (Table 1), conditions of clear-skies and light surface wind during the day favored SB circulation in the MRSP early afternoon (1200–1400 LT), changing the direction of surface wind to southeast, increasing moisture and decreasing temperature. The mean values of sunshine duration, sky cover and net radiation during these days were, respectively, 8 ± 0.8 hr, 4.2 ± 1 okta and -351 ± 41 W m^{-2} (Table 1). However, during summer SB circulation contributes to increase cloud activity during the afternoon in the MRSP. Even though this mesoscale disturbance increases cloudiness in the afternoon, and in some cases producing rain, it subsided during nighttime, and the sky becomes progressively clear favoring the development of LLJ. A good example of this recovering is the LLJ event on 24–25 February. Although this LLJ event was associated to the UTCV, the passage of SB front during the afternoon on 24 February increased cloudiness, producing 14.7 mm of rain in the MRSP (Table 1). Nevertheless, cloud cover dissipated during the night and clear-sky conditions associated to the UTCV prevailed, favoring the development of LLJ in the MRSP. In this event, the LLJ formed at 2100 LT on 24 February, lasted for 18 hr until 1500 LT of 25 February. The synergy between SB circulation and LLJ will be analyzed in more details in the Section 5.3. Should be emphasized that hourly values of wind speed and direction measured in the PEFI and IAG are well correlated. During the day, Pearson's correlation coefficients are equal to 0.54 and 0.98. During the night, they reached 0.8 and 0.72, respectively. This shows that the wind speed and direction measured in the PEFI, and used in this section to identify the presence of SB, can be considered representative of the MRSP.

5.1.2. Winter Campaign

5.1.2.1. Synoptic Scale Systems

Similarly, favorable synoptic scale conditions prevailed on six out of 10 nights and LLJ events occurred in eight nights during the winter field campaign (Figure 5b). The LLJ events observed under clear-sky (three) conditions on the nights of 6–7, 7–8, and 12–13 August were associated to subsidence induced by a SASH. During nighttime period the mean values of sky cover and net radiation were, respectively, 0 okta and 64 ± 3 W m^{-2} (Table 2). These LLJs displayed a maximum intensity varying from 5.8 to 12.8 m s^{-1}, occurring between 0300 and 0900 LT, blowing from northeast quadrant and between 156 and 515 m. They started between 1800 and 0300 LT and lasted from 9 to 18 hr (Table 2).

Three LLJ events observed in partially cloudy conditions on the nights of 8–9, 9–10, and 11–12 August were associated with SASH (first two) and HPS-induced subsidence. During these nights the mean values of sky cover and net radiation were, respectively, 4.6 ± 0.8 okta and 64 ± 2 W m^{-2} (Table 2). On the nights of August 8–9 and 9–10, the subsidence was progressively reduced by a CF, which reached the RMSP on 11 August. LLJ event of 11–12 August occurred under synoptic conditions associated with a post-frontal HPS moving northeast and merging, progressively, with the semi stationary SASH, producing surface anticyclonic circulation and subsidence. These LLJs displayed a maximum intensity varying from 11.0 to 14.8 m s^{-1}, between 0600 and 0900 LT, from north-northwest sector and between 414 and 780 m. They started between 2100 and 0300 LT and lasted from 6 to 12 hr (Table 2).

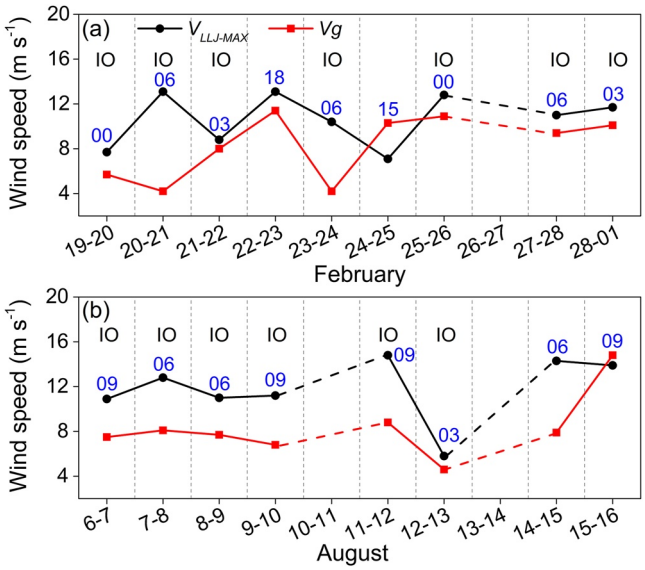

Figure 6. Time evolution of maximum low-level jet (LLJ) intensity ($V_{LLJ-MAX}$) and correspondent geostrophic wind (Vg) during (a) 19–28 February and (b) 6–15 August 2013 on the metropolitan region of São Paulo. The symbol IO indicates to LLJ events associated with the inertial oscillation mechanism according to the wind hodographs. The dashed black lines indicate absence of nighttime LLJ. Numbers indicate 0000, 0300, 0600, 0900, 1500, and 1800 LT and correspond to the time when the LLJ event reaches the maximum intensity.

In the night of 13–14 August, the meteorological conditions in the MRSP were severely disturbed by the passage of another CF. As consequence, surface wind speed increases and no LLJ was observed.

The LLJ events observed in the nights of 14–15 and 15–16 August occurred under cloudy conditions resulting from the passage of the CF in the previous day. During these two nights the mean values of sky cover and net radiation were, respectively, 8 okta and 30 W m^{-2} (Table 2). The event of 14–15 August was induced by the baroclinicity associated to the CF (Nair et al., 2004). It reached maximum intensity of 14.3 m s^{-1} at 0600 LT and 955 m, with direction from south, starting at 2100 LT and lasting 9 hr (Table 2). On the other hand, the LLJ event on 15–16 August was associated to the post-frontal HPS moving away from the MRSP. It reached maximum intensity of 13.9 m s^{-1} at 0900 LT and 545 m, with direction from east-northeast. It started at 0300 LT and lasted for 6 hr (Table 2).

5.1.2.2. Mesoscale System

In average, frequency of SB-event oscillates around 50% and it does not vary significantly during the year in the MRSP (Oliveira et al., 2003). The frequency of SB during field campaigns of 2013 deviated partially from the above behavior, because only one SB event was detected in August (Table 2) and five in February campaign (Table 1).

The deviation during field campaign of August 2013 occurred because winds from north-northwest sector induced by the anticyclonic circulation of the SASH, which was closer to the South American continent, prevented the southeast winds of the SB from reaching the MRSP. Cloudy conditions induced by the passage of CFs prevailed during 11, 14, and 15 August, significantly inhibited the land-ocean thermal contrast and, therefore SB development. As it will be discussed in detail in Section 5.3, the SB on 6 August was strong and, as in the summer cases, induced a LLJ that reached a maximum at the end of the afternoon as the SB subsided, only to intensify again after mid-night at lower heights reaching a maximum intensity at 0900 LT the following day.

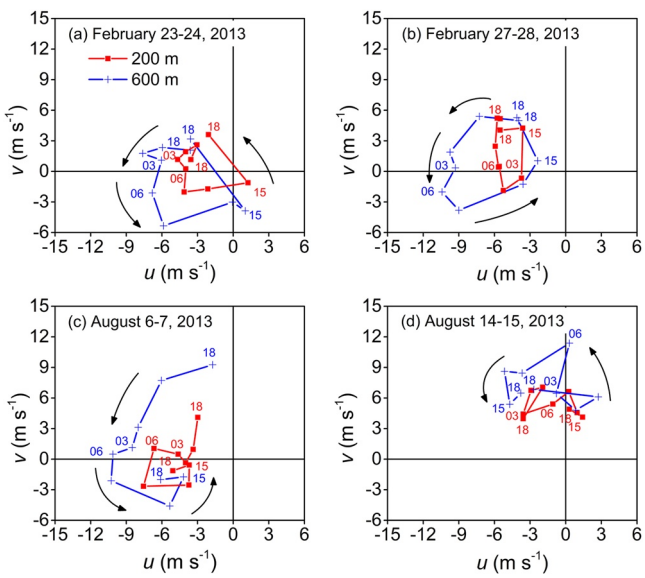

Figure 7. Wind hodographs based on rawinsonde wind values interpolated at 200 (red) and 600 m (blue) for (a) 23–24 February, (b) 27–28 February, (c) 6–7 August and (d) 14–15 August 2013, on the MRSP. Numbers indicate 0300, 0600, 1500, and 1800 LT.

5.2. The Role of Inertial Oscillation on the LLJ Formation

According to Blackadar's theory, the inertial oscillation mechanism is present in the formation of the LLJ ever that its intensity becomes greater than geostrophic wind velocity. The LLJ associated to this super geostrophic flow reaches its maximum intensity in a time equal to half of the inertial oscillation period. As another consequence of inertial oscillation, the trajectory described by the wind vectors rotates clockwise (counterclockwise) at the LLJ height in the northern (southern) hemisphere. Even though, in the real atmosphere there are situations liked documented by Chimonas (2005) when, due to the influence of secondary circulations, the observed period of oscillation does not coincide with the one predicted by Blackadar's theory. The presence of super geostrophic flow and clockwise rotation has been used to diagnosticate the presence of inertial oscillation as the main mechanism of LLJ formation (Markowski & Richardson, 2011). In this work the presence of super geostrophic flow (Figure 6) and counterclockwise rotation (Figure 7) will be used as indication of the inertial oscillation mechanism in the formation of the LLJs observed in the MRSP.

As indicated in the Figure 6, about 88.2% (15 of 17) of LLJ events display super geostrophic intensity. The 86.6% of these LLJ events show a counterclockwise rotation typical of inertial oscillation mechanism and 60% reaching maximum intensity between 0600 LT and 0900 LT. This likewise confirms

the Blackadar predictions of LLJ maximum intensity taking place about half of the inertial period during the most super geostrophic LLJ events. In the case of São Paulo (~23.5°S) it corresponds to ~15 hr.

The MRSP was not significantly affected by synoptic disturbances during the most days with super geostrophic LLJs. Besides, during these days the MRSP was influenced by large-scale meteorological conditions, such as UTCV and SASH (Figure 5), that inhibits clouds and induced light surface winds. However, wind hodographs during super geostrophic LLJ event on 22–23 February and 14–15 August (Figure 7d) do not show a clear counterclockwise rotation typical of inertial oscillation mechanism. These two LLJ events occurred during disturbed conditions due to the passage of a shortwave UAT during 22–23 February and a CF during 13–14 August (Figure 5).

On the other hand, sub geostrophic LLJ event in the night on 15–16 August occurred during cloudy conditions caused by the proximity of a post-frontal HPS. The sub geostrophic LLJ event in the night on 24–25 February is the only exception because it occurs during undisturbed conditions. As explained in Section 5.1.1.1, during 24 February the cloudy and precipitation conditions associated with the SB passage by the MRSP lasted until midnight. As consequence, no clear inertial oscillation in the wind hodograph was observed.

Figure 7 presents the wind hodographs based on rawinsondes data interpolated linearly at 200 and 600 m during LLJ events observed in summer (23–24 February and 27–28 February) and winter (6–7 August and 14–15 August) field campaigns of 2013. A counterclockwise rotation is observed during LLJ events of 23–24, 27–28 February, and August 6–7 in both levels, indicating inertial oscillation, mainly at 600 m. Similar results were obtained by Barlow et al. (2015) in London, UK, using lidar and Ruchith and Raj (2015) in Pune, India, using Doppler lidar. According to Barlow et al. (2015), in urban areas the inertial oscillation is most clear above the LLJ because roughness and surface heating disrupt the LLJ structure below. Results obtained by Baas et al. (2009) showed that inertial oscillation is also the main mechanism of LLJs formation in the rural site of Cabauw. It is important to note that inertial oscillation is not always present. When the decoupling of the air above the SIL is not strong enough, inertial oscillation is not observed (Baas et al., 2009). In the latter case, mesoscale and synoptic disturbances may inhibit inertial oscillation (Baas et al., 2009; Kallistratova & Kouznetsov, 2012; Lundquist, 2003). During disturbed LLJ event of 14–15 August no clear counterclockwise rotation was observed, corroborating the last affirmation (Figure 7d).

Despite the low latitude of São Paulo (23.5°S), inertial oscillation seems to be the main mechanism that originates LLJs in the MRSP. Approximately 76.4% of the LLJ events observed during the field campaigns (seven in summer and six in winter) display inertial oscillation mechanism features, such as counterclockwise rotation of ageostrophic wind and super geostrophic intensity during nighttime and morning of next day. These features are particularly well defined under synoptic conditions that inhibit cloud and favor light surface winds in the MRSP. The 35.3% of LLJ events occur at nights subsequences to days with SB circulation. Favored by the same synoptic conditions, SB circulation indicated the presence of a mesoscale baroclinicity induced by the land-ocean thermal contrast that may contribute to the formation of LLJs in the MRSP. Given the high frequency of LLJ events (77.6% accordingly this work) and SB events (more than 50% accordingly to Oliveira et al., 2003), it seems plausible to consider simultaneous events as typical feature in the MRSP, as described in the next subsection.

5.3. The Role of SB on the LLJ Formation

To study the role of SB on the LLJ formation in the MRSP, the period 6–7 August 2013, was chosen, where both phenomena were present (Figure 8). The corresponding synoptic surface maps (not shown) show an anticyclonic circulation and subsidence induced by the combination of semi-permanent SASH and a merging migratory HPS. This synoptic condition yielded clear-skies and light surface easterly winds, favoring the formation of a SB during day and LLJ event at night in the MRSP (Figure 5b).

On 6 August, the LLJ appears around 1800 LT at 700 m with intensity of 10.5 m s^{-1} and direction from southeast (Figure 8a). This LLJ event was triggered by the passage of a SB front by the MRSP early in the afternoon, indicated by wind direction shift from northwest to south in the first 700 m between 1200 and 1500 LT (Figure 8a). As indicated by Ribeiro et al. (2018), the passage of SB front in the MRSP disrupt the convective turbulent mixing by increasing thermal stability, inhibiting or even reducing the time evolution of UBL height in the afternoon. In the case of the 6 August, the stabilization resulted in the speeding up the flow at 700 m, producing a

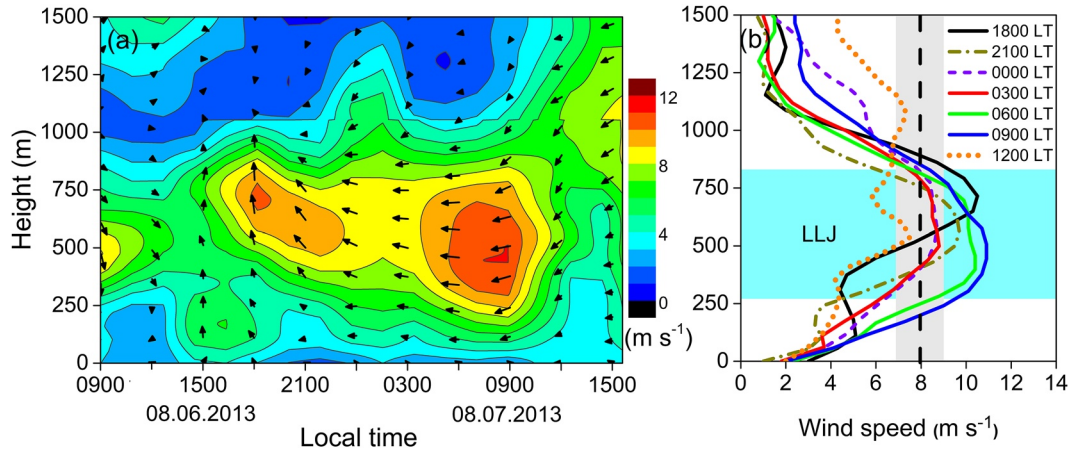

Figure 8. Time evolution of (a) wind speed (color map) and direction (wind vectors) and (b) vertical wind-speed profiles based on rawinsonde carried out in the metropolitan region of São Paulo from 1800 LT on 6 August to 1200 LT on 7, 2013. Black arrows in (a) show wind vector. Vertical dashed black line in (b) indicates mean geostrophic wind speed between 1800 LT of 6 August and 1200 LT of 7 August. Horizontal (cyan) and vertical (gray) strips in (b) indicate, respectively, the range of low-level jet heights and statistic error of the mean geostrophic wind.

super geostrophic LLJ at 1800 LT. The LLJ intensity and height decreases, respectively, to 8.7 m s^{-1} and 580 m around 0000 LT, staying relatively constant up to 0400 LT. At the end of dawn, the LLJ intensifies at low heights (~450 m), reaching 10.9 m s^{-1} from the east-northeast at 0900 LT (Figures 8a and 8b).

During this event, the mean geostrophic wind speed was 8.04 ± 1.05 m s^{-1} at the LLJ height (vertical dashed black line and gray band in Figure 8b), showing that the flow was super geostrophic at 1800 LT, 2100 LT and after 0300 LT. Given the fact that inertial oscillation requires some time to produce LLJ, the super geostrophic flow observed between 1800 and 2100 LT is more likely a result of the passage of SB front. Only at 1200 LT the wind becomes sub geostrophic. During daytime on 7 August, the LLJ core was completely removed by turbulent mixing induced by thermal convection, keeping the wind sub geostrophic in the Mixing Layer during the rest of the daytime.

The presence of super geostrophic (Figure 8b) and counterclockwise rotation (Figure 7c) suggest that a LLJ event results from inertial oscillation mechanism, mainly after midnight. Besides, it is plausible to infer that the passage of SB front by the MRSP is followed by a wind direction shift from northwest to southeast around 1500 LT (Figure 8a), set up the stage for the evening LLJ event by cooling and moistening the atmosphere and setting up a thermal inversion layer at lower levels strong enough to reduce turbulence and decouple the flow above. As consequence, a southeasterly LLJ appears in the second half of the afternoon, reached maximum intensity at ~1800 LT (Figure 8a). As the SB circulation dies out and the sky becomes clear a new shallow SIL, created by the surface radiative cooling, deepens with time and the flow aloft starts again to speed up, as it decouples from the surface, forming a new maximum in the vertical wind speed profile in the MRSP. This easterly LLJ reaches its maximum intensity (10.9 m s^{-1}) in the morning of the next day (Figure 8a).

The wind vector map at 875 hPa (~550 m) at 0900 LT on 7 August 2013, obtained from ERA5 reanalysis (Section 3.3), corresponds to a horizontal domain of 4° (~444 km) by 3° (~333 km) around the MRSP (green rectangle), is indicated in Figure 9a. The geostrophic wind vectors (red arrow) are aligned parallel to the geopotential lines (blue lines). Due to friction, the actual wind vectors (black arrow) point to the geostrophic wind right as expected for the Southern Hemisphere. Inside the MRSP (green rectangle in Figure 9a) the actual wind intensity is super geostrophic. The vertical distributions of actual and geostrophic winds between 925 and 800 hPa during initial phase of the LLJ event indicate a sub geostrophic flow (Figure 9b). At LLJ level (green-contour gray rectangle), the actual flow (black arrow) progressively shifts from sub to super geostrophic during nighttime as it turns from southeast to east-northeast (Figure 9b). The time evolution of the actual wind from ERA5 confirmed the pattern display in the Figure 8.

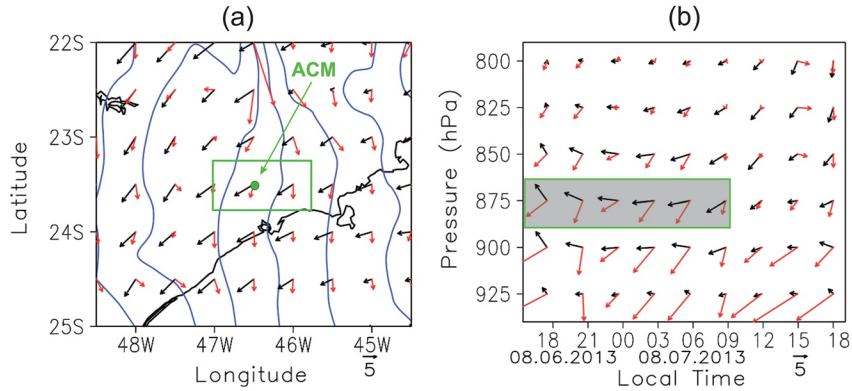

Figure 9. (a) Wind vector map at 875 hPa (~550 m) at 0900 LT on 7 August 2013; (b) Vertical distribution of wind vector during 6–7 August 2013, at the "*Campo de Marte*" Airport (ACM), provided by ERA5 reanalysis. The actual wind is indicated by black arrow and geostrophic wind by red arrow. In (a) blue lines indicate the 875 hPa geopotential heights, green rectangle corresponds to the metropolitan region of São Paulo and green solid circle to ACM. The wind scale reference is indicated by arrow on the top of 5 and correspond to 5 m s^{-1}. Green-contour gray rectangle emphasize time evolution of actual (black arrow) and geostrophic (red arrow) wind at 875 hPa from 1800 to 0900 LT at ACM.

5.4. LLJ Interactions With UHI, SIL, and Pollution

Relations among LLJ and UHI, SIL, pollutants concentration in the MRSP are illustrated in Figure 10. The UHI intensity is estimated based on surface observation described in Section 3.2. The SIL strength was estimated from rawinsondes data by $\Delta\theta_{SIL}/Z_{SIL}$, where $\Delta\theta_{SIL} = \theta(Z_{SIL}) - \theta_0$, $\theta(Z_{SIL})$ and θ_0 are the potential temperatures at the SIL top (Z_{SIL}) and surface, respectively (Sánchez et al., 2020). Pollutants analyzed here correspond to $PM_{2.5}$ and CO described in Section 3.4.

The LLJ and UHI intensities are negatively correlated (Figures 10a and 10b), with Pearson's coefficient $r = -0.74$, showing that LLJ inhibits the UHI intensity in the MRSP. The corresponding determination coefficient ($R^2 = 0.54$) shows that 54% of the observed variability in UHI intensity is associated to the ventilation effect, causing vertical mixing induced by wind shear below the LLJ core. Similar negative correlation ($r = -0.81$) between LLJ and UHI intensities was also observed in Oklahoma City, USA, by Hu, Klein, Xue, Lundquist, et al. (2013), indicating that ventilation effect associated to LLJ diminish UHI intensity in urban areas.

The LLJ intensity and SIL strength are also negatively correlated (Figures 10c and 10d), with $r = -0.76$, indicating that LLJ inhibits SIL strength. The corresponding determination coefficient ($R^2 = 0.58$) shows that ventilation effect induced by the LLJ does also handle most of the SIL-strength variation in the MRSP.

Besides ventilation, LLJs have other effects on the UHI and UBL during nighttime. Hu, Klein, Xue, Lundquist, et al. (2013) verified that the heat released in the surface by the urban canopy is mixed through the UBL and transported horizontally by the LLJ to the neighboring rural areas of Oklahoma, USA. This transport diminishes the UHI intensity by expanding it horizontally. They also verified strong LLJ increases vertical mixing allowing for a deeper and less stable nocturnal boundary layer and a weaker surface radiational cooling at the rural areas surrounding Oklahoma City. The strong correlations found in this study suggest that the above mentioned LLJ effects observed in Oklahoma may also be acting on MRSP, playing an important role in modulating the UHI intensity and SIL strength in both urban and rural portions of the MRSP.

Figures 10e–10h displays the correlation among LLJ and pollutants concentration at the surface ($PM_{2.5}$, CO) in the MRSP. The LLJ intensity is negatively correlated with the $PM_{2.5}$ and CO, with $r = -0.72$ and -0.80, respectively. This shows that LLJ-ventilation effect may be contributing to dilute pollutants concentrations in the surface of the MRSP during nighttime. Moreover, nighttime horizontal advection associated with LLJ may be also contributing to further reduce $PM_{2.5}$ and CO in the MRSP by bringing in more pristine air from less polluted rural areas. Miao et al. (2019) verified that the occurrence of LLJ favors the dilution of $PM_{2.5}$ over Beijing, China.

5.5. Seasonal Variation of the LLJ Properties

During the MCITY period, the LLJs occur most often between 2100 LT and 0900 LT (Figure 11a). This shows that LLJs in the MRSP can be considered a nocturnal phenomenon. During the regular-sounding period, it

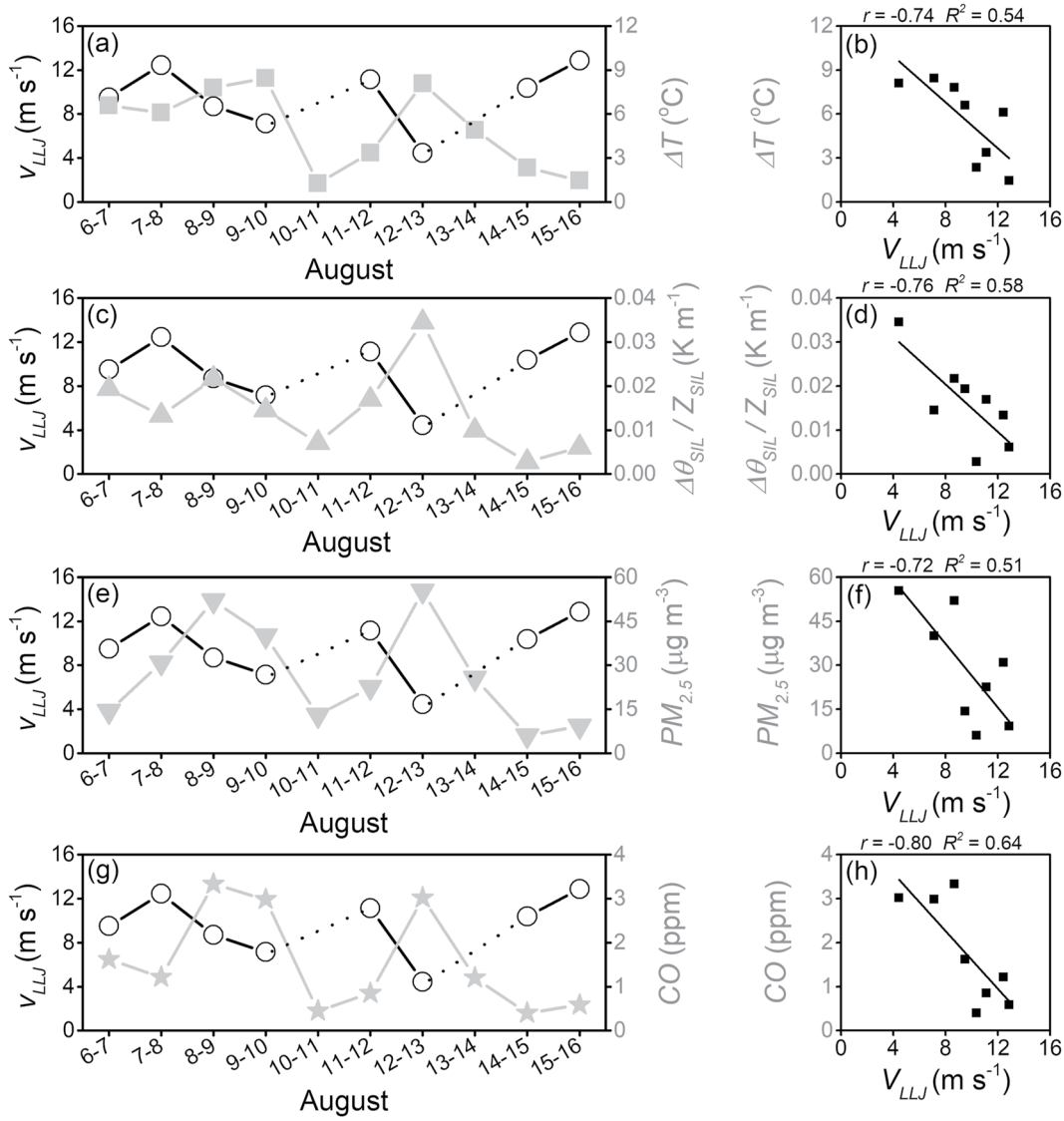

Figure 10. Time evolution and dispersion diagram of low-level jet (LLJ) intensity (V_{LLJ}) and (a–b) urban heat island intensity (ΔT), (c–d) surface inversion layer (SIL) strength ($\Delta\theta_{SIL}/z_{SIL}$), (e–f) particular matter 2.5 ($PM_{2.5}$), and (g–h) carbon monoxide (CO) observed in the metropolitan region of São Paulo during the winter field campaign in August 2013. Average values during LLJ duration time. The dashed black lines in (a), (c), (e) and (g) indicate nighttime absence of LLJ.

was identified LLJs in 63.2% (836 of 1,323) of soundings at 0900 LT and 63.4% (816 of 1,288) at 2100 LT (Figure 11b). During MCITY periods, LLJ events are identified in 60% (12 of 20) of soundings at 0900 LT and 50% (10 of 20) at 2100 LT.

About 78.8% of LLJs (63 soundings) detected during MCITY periods and 84% (1,391 soundings) detected during regular-soundings period have intensities ranging between 4 and 12 m s^{-1} (Figures 11c and 11d). They correspond to mean intensities of 8.5 ± 0.3 m s^{-1} and 7.8 ± 0.1 m s^{-1}, respectively. During MCITY periods, LLJ-heights range from 95 to 962 m, with the largest frequency (31 soundings) in the class of 450–750 m and mean height equal to 539 ± 26 m (Figure 11e). During regular-soundings period, the LLJs display higher frequency in the LLJ-heights class (778 soundings, 450–750 m) that is equal to the MCITY period soundings (Figure 11f). However, LLJs in the regular-sounding period have higher mean height (640 ± 151 m).

These results reveal that the LLJs in the MRSP have properties (height and intensity) like ones observed in other locations such as: North Florida, USA; Colima Valley, Mexico; Moscow, Russia; Yangtze River Delta, China; Pune, India and Cabauw, Netherlands (Table 3). On the other hand, the LLJ in the MRSP is as frequent as in

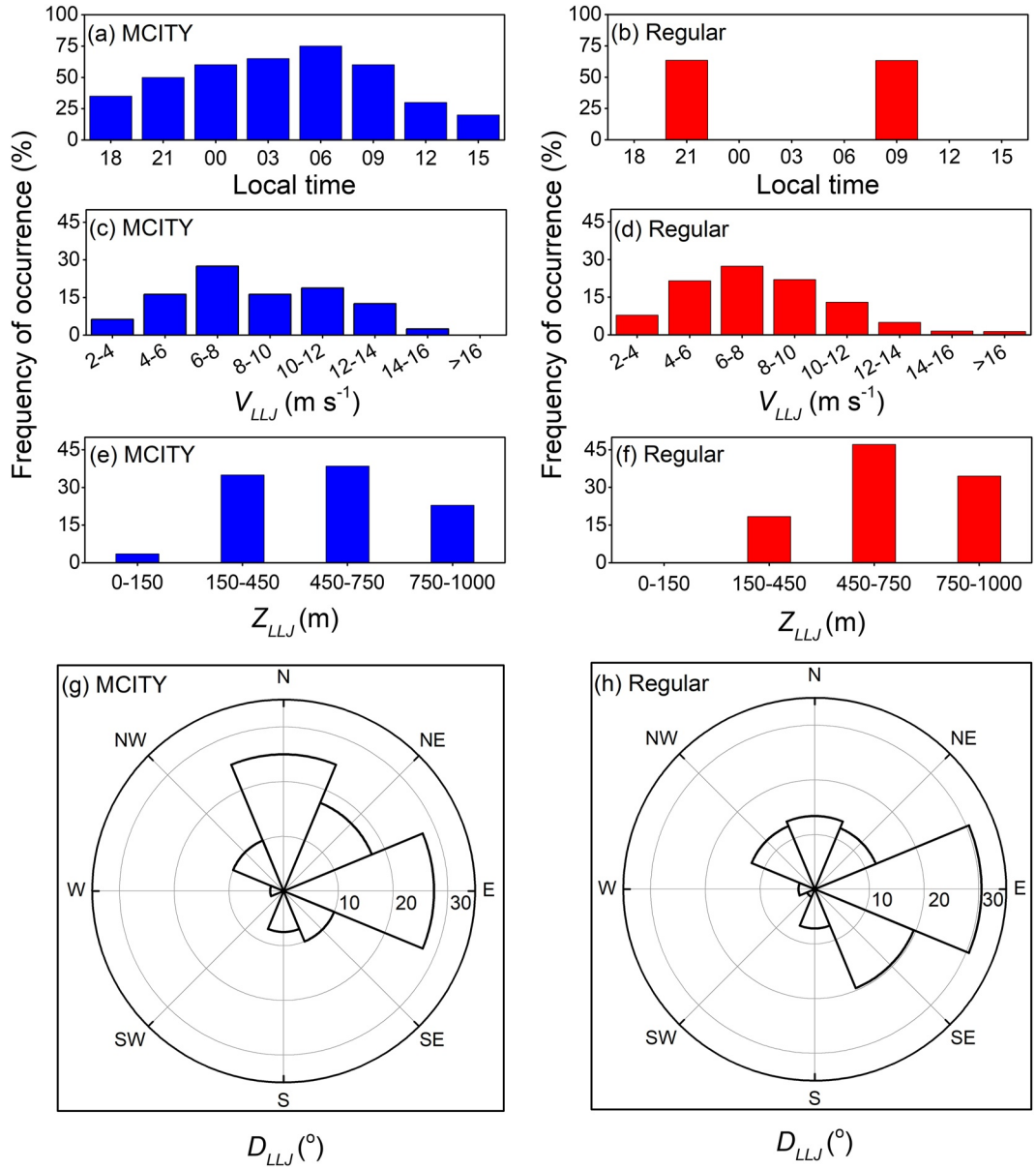

Figure 11. Histogram of low-level jet (LLJ) (a)–(b) hourly frequency; (c)–(d) intensity; (e)–(f) height; and (g)–(h) direction, based on fine (MCITY) and coarse (regular) resolution rawinsondes carried out, respectively, during summer and winter fields campaigns of 2013, and from 2009 to 2013 in the metropolitan region of São Paulo. The hourly frequency corresponds to number of LLJ divided by total number of soundings in every hour.

Colima Valley, Mexico; Yangtze River Delta, China; and both Great Plains and North Florida in the USA. Only the LLJs in Cabauw, Netherlands and Pune, India, are less frequent than in the MRSP. Considering urban areas, the LLJ in the MRSP is as frequent as in Moscow, and more frequent than in Hannover, Germany.

During both MCITY and regular periods the predominant LLJ-direction is east with frequency of 27.5% and 30.5%, respectively (Figures 11g and 11h). The second most frequent direction is north with 25% for MCITY (Figure 11g) and southeast with 19.6% for regular period (Figure 11h). This apparent discrepancy seems to be related to the fact that in the regular-sounding period there are soundings only at 0900 and 2100 LT. Therefore, soundings only at these hours do not provide as much information about LLJ direction as every 3-hr soundings carried out in the MCITY periods. The LLJ direction predominance in the MRSP can be explained in terms of inertial oscillation. Under undisturbed conditions the northeast LLJ occurs as the east wind vector oscillated

Table 3
Low-Level Jet (LLJ) Properties Worldwide

	LLJ				Data set		
Local	Freq. (%)	Intensity (m s^{-1})	Height (m)	Land use	Size	Resolution (m)	Sounding
MRSP, Brazil[a]	85 (77.6)	8.5 ± 0.3 (7.8 ± 0.1)	539 ± 26 (640 ± 151)	Urban	20 days (4 years)	62 (302)	Rawinsonde
Kansas, USA (Song et al., 2005)	63	10–30	200–400	Rural	6 years	5 60	Minisodars Wind profilers
North Florida, USA (Karipot et al., 2009)	62	6–14	100–500	Rural	2 years	20	Doppler sodar
Cabauw, Netherlands (Baas et al., 2009)	20	6–10	140–260	Rural	7 years	60	Wind profiler
Moscow, Russia (Kallistratova & Kouznetsov, 2012)	69	2–12	50–450	Urban Rural	27 days	20	Doppler sodar
Yangtze River Delta, China (Wei et al., 2013)	77	6–14	400–600	Rural	1 year	50	Wind-profile radar
Hannover, Germany (Emeis, 2014b)	21	7–23	150–650	Urban	2 years	25	Sodar
Pune, India (Ruchith & Raj, 2015)	42	5–11	300–900	Rural	2 years	50	Doppler lidar
Colima Valley, Mexico (Arfeuille et al., 2015)	88	11.7 ± 2.3	308 ± 160	Rural	504 days	10	Sodar-RASS

[a]MCITY (regular) rawinsonde.

inertially around northeast geostrophic wind (red arrow in Figure 9), occurring in undisturbed conditions associated to the presence of semi-permanent SASH over the Atlantic Ocean (Figure 1). LLJ from southeast can be explained by the passage of SB front by the MRSP (Section 5.3). Similarly, more intense and higher southeasterly LLJs are associated with post-frontal conditions due to the passage of CF by the MRSP. As observed by Karipot et al. (2009) in Florida, USA, the large pressure gradients related to the CF passage can influence the formation of strong LLJs. The inspection of synoptic map (not shown) indicates that 17.6% of LLJ events observed in the MRSP are associated to CF and post-frontal HPS associated during the field campaigns.

Figure 12 presents the seasonal variation of frequency of daily LLJ events, intensity, height, and wind direction of the LLJs in the MRSP based on the regular-sounding period. In this case a LLJ event is considered when: (a) it is detected simultaneously at 2100 LT and at 0900 LT of the next day; (b) it is detected at 2100 LT, and it is not detected at 0900 LT of the next day; (c) it is detected at 0900 LT, and it is not detected at 2100 LT of the night before. Based on Figure 12a is possible to infer that the LLJ is a persistent climate feature of the MRSP, occurring at least in 70% of days in all months with annual average of 77.6 ± 1%. The amplitude of the seasonal variation of LLJ occurrence is small, with highest incidence in December (85.5%) and lowest in June (70%).

Like frequency, monthly values of LLJs intensity and height do also display small seasonal variation (Figure 12). From July to October the LLJ is slightly more intense, varying from a minimum of 7.1 ± 0.2 m s^{-1} in February to a maximum of 8.6 ± 0.3 m s^{-1} in October (Figure 12b). During summer and autumn months (November to May) the LLJs occur at slightly higher heights, varying from maximum of 703 ± 151 m in March to a minimum of 577 ± 151 m in June (Figure 12c).

The seasonal variation of LLJ intensity (height) is associated with the patterns of SB circulation, which is more intense during spring months (September to November) in the MRSP, when the land-ocean thermal contrast goes through a maximum due to the fact that ocean takes more time to respond to the seasonal increase of solar radiation heating than the land (Sánchez et al., 2020). On the other hand, seasonal variation of LLJ frequency seems to respond seasonal variation of solar radiation with a maximum in summer (December) and minimum in winter (July).

Wind direction at the jet core shows a more complex seasonal variation in the MRSP (Figure 12d). The predominant direction is east from March to December (32.3 ± 2%), southeast in January (23%) and north in February (27%). Based on how meso and large-scale systems affect LLJs in the MRSP, described in the previous sections, seems plausible to associate seasonal variation of predominant direction to (a) seasonal variation in the position of the SASH, (b) intensification of SB circulation, and (c) increase in the frequency of CF during winter and

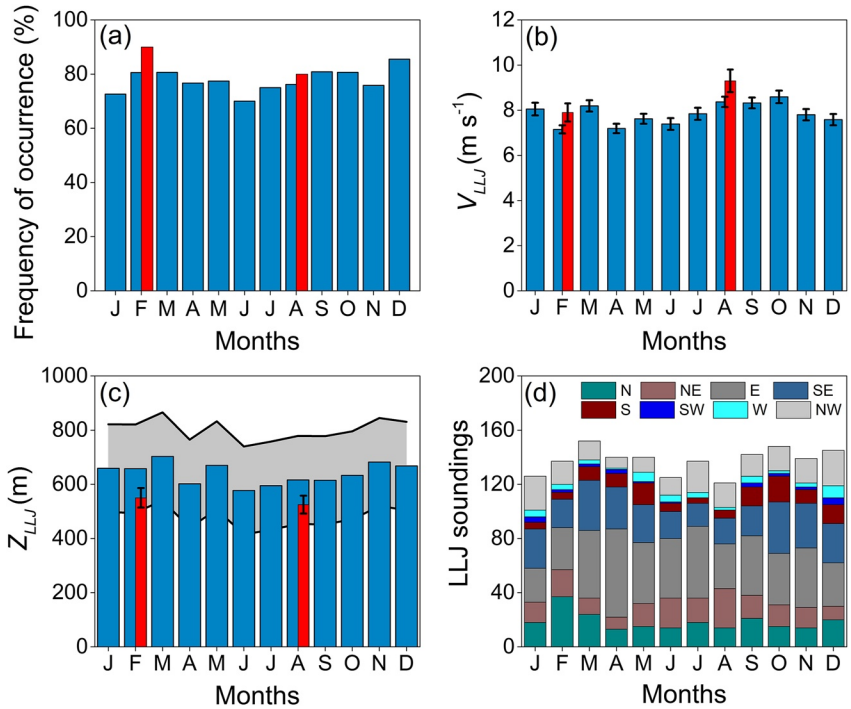

Figure 12. Seasonal variation of (a) frequency of daily low-level jet (LLJ) events, (b) intensity, (c) height and (d) wind direction of LLJ in the metropolitan region of São Paulo from September 2009 to August 2013 (Regular rawinsondes). The vertical red column in (a)–(c) refers to field campaigns of 2013. The statistical errors are indicated by the vertical bars in (b). Uncertainty due to the resolution of 62 m (MCITY) and 302 m (Regular) is indicated, respectively, by vertical bars and horizontal gray strip in (c).

spring months (de Jesus et al., 2016). The interactions among LLJ, synoptic and local circulations are quite complex and require using numerical models to be properly addressed. The numerical investigation of these interactions will be undertaken in a future work.

6. Conclusion

In this work, the main features of LLJ in the MRSP are described using 160 fine-resolution (62 m) rawinsondes, carried out every three hours during 20 days in the summer (19–28 February) and winter (6–15 August) MCITY BRAZIL Project campaigns of 2013, and 2611 coarse resolution (302 m) rawinsondes carried out regularly twice a day at 0900 LT and 2100 LT from 1 September 2009, to 16 August 2013.

The new algorithm, developed to identify LLJs in the MRSP, is well suited to retrieve LLJ height, intensity and direction in both fine and coarse-resolution soundings. It retrieves LLJ height with uncertainties of ±31 and ±151 m, respectively in fine and coarse resolution soundings. The impact of vertical resolution on LLJ intensity and direction are smaller because in average the width of LLJs observed in the MRSP is 816.9 ± 36 m, more than the twice resolution of the coarse-resolution soundings.

The analysis of 160 fine-resolution rawinsondes indicated that during summer field campaign of February 2013, LLJ events were observed in nine out of 10 nights. Seven occurred during clear-sky or partially cloudy conditions induced by the subsidence associated to UTCV positioned northeast of the MRSP. Two occurred under cloudy conditions induced by the influence of a shortwave UAT.

During winter campaign of 2013, LLJ events were observed in eight out of 10 nights. Six events occurred under clear-sky or partially cloudy conditions induced by subsidence associated to SASH (five) and post-frontal HPS merging to SASH (one). Both synoptic patterns cause light surface winds from northwest to northeast quadrants and east-southeast sector in the MRSP. Two events occurred under cloudy conditions triggered by the passage of CF and the post-frontal HPS moving away from the MRSP, that induce high surface winds from southeast.

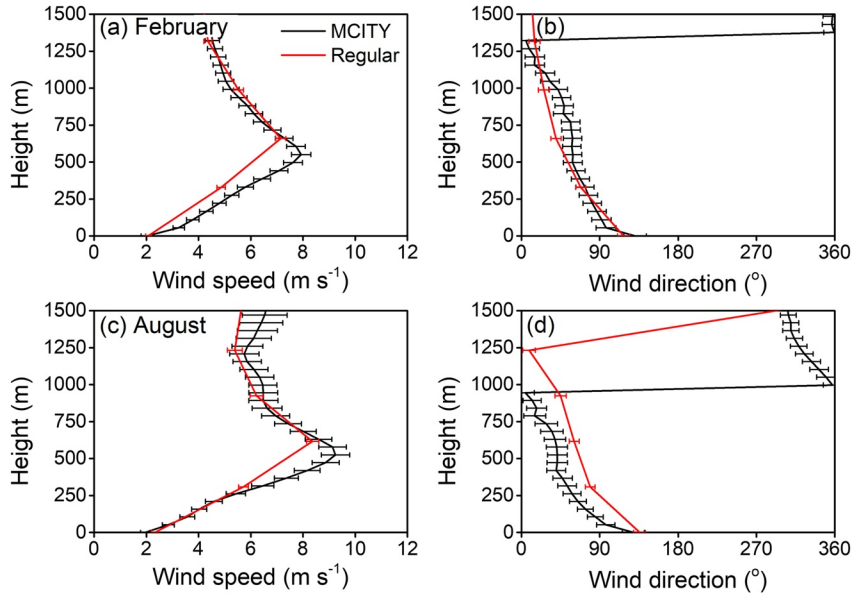

Figure 13. Seasonal variation of low-level jet (LLJ) vertical structure average during February and August. Vertical profiles of (a)–(c) wind speed and (b)–(d) wind direction are estimated using MCITY and Regular rawinsondes carried out in the MRSP from September 2009 to August 2013. The statistical errors are indicated by the horizontal bars.

Clear-sky conditions and light surface wind also favor the SB circulation observed, simultaneously to the LLJ events, in six out of 20 days of field campaigns, indicating a link between these two phenomena in the MRSP. It seems reasonable to assume that mesoscale baroclinicity associated to land-ocean thermal contrast induces direct southeast-flow that generates northeast secondary flow that, during nighttime, decouples from the surface and oscillates inertially. Similar mechanism has been observed in other coastline area such as Cabo Frio (Ribeiro et al., 2016), located approximately 500 km far from São Paulo City, suggesting that LLJ observed in the MRSP is part of a broader event.

Spite the low latitude (~23.5°S), counterclockwise rotation and super geostrophic intensity presented by LLJ events in the absence of any significant synoptic disturbances suggests that inertial oscillation is the dominant formation mechanism of the LLJs in the MRSP.

It was found that LLJ are negatively correlated with UHI and SIL in the MRSP, with correlation coefficient −0.74 and −0.76, respectively. Given the fact that meteorological conditions favoring LLJ do also favor UHI and SIL strength, it is hypothesized that turbulent mixing induced by the LLJ contributes to inhibit the intensification of UHI and SIL. LLJ is also negatively correlated with $PM_{2.5}$ and CO concentration, indicating that it plays an important role in the dilution of these pollutants in São Paulo megacity.

The analysis of 2611 coarse resolution rawinsondes indicated that from the climatological point of view, the LLJs have a high frequency throughout the year in the MRSP, with a maximum in December (85.5% of days) and the minimum in June (70% of days). The LLJ speed and height show a small seasonal variation with mean intensity of 7.8 ± 0.1 m s^{-1} and height of 640 ± 151 m. The largest frequency of LLJ directions is from east (30.5%) and southeast (19.6%). The frequency of LLJ events in February (80.5% of days) and in August (76.1% of days) are smaller than in the field campaigns of February (90% of days) and August (80% of days) of 2013. The mean LLJ speed in February (7.2 ± 0.2 m s^{-1}) and August (8.4 ± 0.2 m s^{-1}) are smaller than in the field campaigns of February (7.9 ± 0.4 m s^{-1}) and August (9.3 ± 0.5 m s^{-1}) of 2013. On the other hand, the mean LLJ height in February (658 ± 151 m) and August (616 ± 151 m) are higher than in the field campaigns of February (550 ± 31 m) and August (525 ± 31 m) of 2013. Figure 13 confirm that the mean vertical structure of the LLJ in the MRSP is a robust feature of the local climate, found in both fine (MCITY) and coarse (Regular) resolution soundings. Differences between MCITY and Regular mean profiles are because MCITY soundings has a large temporal resolution (every 3-hr) but covering small period span (10 days).

The main conclusion of this work is that LLJ events occur in 85% of the days during the MCITY-sounding periods (20 days) and in 77.6% of the days during regular-soundings period (1,446 days). LLJ events are

observed at nighttime in 80% of the days during the MCITY field campaigns and in 56.2% of the days during regular-sounding period. The intensity and height of the LLJs observed in São Paulo are mostly found in the range of $4 \leq V_{LLJ} \leq 12$ m s^{-1} and 450 ± 151 m $\leq Z_{LLJ} \leq 750 \pm 151$ m, respectively. The LLJs direction is predominantly from east. These results are consistent with the earlier analysis performed by Sánchez et al. (2020) using a subjective method to find LLJ events in the MCITY field campaigns soundings of 2013.

The objective analysis performed in the present study and results obtained previously by Sánchez et al. (2020) have showed that coarse resolution soundings can be used to identify LLJ events along with their properties (intensity, height and direction) as well to estimate the UBL structure (maximum daytime height and nighttime residual layer top). Therefore, the algorithms developed in both works can be used to extend UBL climatology to a larger number rawinsondes stations and carried out during a longer period, available (but unused) in Brazil and other countries' network station.

Data Availability Statement

Datasets, composed of properties of the LLJ, UHI and SIL, are available at https://data.mendeley.com/datasets/gb9d7bxsdb/1. ERA5 data set can be found in https://cds.climate.copernicus.eu/cdsapp#!/dataset/reanalysis-era5-pressure-levels?tab=%20form. Pollutant concentrations data set are available at https://qualar.cetesb.sp.gov.br/qualar/home.do.

Acknowledgments
This research was sponsored by the Brazilian Research Foundations: FAPESP (2011/50178-5; 2020/07141-2), FAPERJ (E26/111.620/2011; E26/103.407/2012), CNPq (309079/2013-6; 305357/2012-3; 462734/2014-5; 304786/2018-7) and CAPES (CAPES 001). The first author acknowledges the scholarship provided by CAPES. We would like to thank the Brazilian Air Force.

References

Alvares, C. A., Stape, J. L., Sentelhas, P. C., De Moraes Gonçalves, J. L., & Sparovek, G. (2014). Köppen's climate classification map for Brazil. *Meteorologische Zeitschrift*, *22*(6), 711–728. https://doi.org/10.1127/0941-2948/2013/0507

Andreas, E. L., Claffey, K. J., & Makshtas, A. P. (2000). Low-level atmospheric jets and inversions over the western Weddell Sea. *Boundary-Layer Meteorology*, *97*(3), 459–486. https://doi.org/10.1023/a:1002793831076

Arfeuille, G., Quintanilla-Montoya, A. L., González, F. C. V., & Villarreal, L. Z. (2015). Observational characteristics of low-level jets in central western Mexico. *Boundary-Layer Meteorology*, *155*(3), 483–500. https://doi.org/10.1007/s10546-015-0005-0

Baas, P., Bosveld, F. C., Baltink, H. K., & Holtslag, A. A. M. (2009). A climatology of nocturnal low-level jets at Cabauw. *Journal of Applied Meteorology and Climatology*, *48*(8), 1627–1642. https://doi.org/10.1175/2009JAMC1965.1

Banta, R. M., Newsom, R. K., Lundquist, J. K., Pichugina, Y. L., Coulter, R. L., & Mahrt, L. D. (2002). Nocturnal low-level jet characteristics over Kansas during CASES-99. *Boundary-Layer Meteorology*, *105*(2), 221–252. https://doi.org/10.1023/a:1019992330866

Banta, R. M., Pichugina, Y. L., Kelley, N. D., Hardesty, R. M., & Brewer, W. A. (2013). Wind energy meteorology: Insight into wind properties in the turbine-rotor layer of the atmosphere from high-resolution Doppler lidar. *Bulletin of the American Meteorological Society*, *94*(6), 883–902. https://doi.org/10.1175/BAMS-D-11-00057.1

Banta, R. M., Senff, C. J., White, A. B., Trainer, M., McNider, R. T., Valante, R. J., et al. (1998). Daytime buildup and nighttime transport of urban ozone in the boundary layer during a stagnation episode. *Journal of Geophysical Research*, *103*(D17), 22519–22544. https://doi.org/10.1029/98JD01020

Barlow, J. F. (2014). Progress in observing and modelling the urban boundary layer. *Urban Climate*, *10*, 216–240. https://doi.org/10.1016/j.uclim.2014.03.011

Barlow, J. F., Halios, C. H., Lane, S. E., & Wood, C. R. (2015). Observations of urban boundary layer structure during a strong urban heat island event. *Environmental Fluid Mechanics*, *15*(2), 373–398. https://doi.org/10.1007/s10652-014-9335-6

Berg, L. K., Riihimaki, L. D., Qian, Y., Yan, H., & Huang, M. (2015). The low-level jet over the southern Great Plains determined from observations and reanalyses and its impact on moisture transport. *Journal of Climate*, *28*(17), 6682–6706. https://doi.org/10.1175/JCLI-D-14-00719.1

Beu, C. M. L. (2019). *Low-level jet study at Iperó with the Doppler lidar technique (Doctoral Thesis)*. Institute of Nuclear Energy Research, University of São Paulo. Retrieved from https://www.researchgate.net/publication/343333283_Estudo%20_do_jato_de_baixos_niveis_em_Ipero_com_a_tecnica_lidar_Doppler

Blackadar, A. K. (1957). Boundary layer wind maxima and their significance for the growth of nocturnal inversions. *Bulletin of the American Meteorological Society*, *38*(5), 283–290. https://doi.org/10.1175/1520-0477-38.5.283

Bonner, W. D. (1968). Climatology of the low level jet. *Monthly Weather Review*, *96*(12), 833–850. https://doi.org/10.1175/1520-0493(1968)096<0833:COTLLJ>2.0.CO;2

Chimonas, G. (2005). The nighttime accelerations of the wind in the boundary layer. *Boundary-Layer Meteorology*, *116*(3), 519–531. https://doi.org/10.1007/s10546-005-0609-x

Corrêa, P. B., Dias-Júnior, C. Q., Cava, D., Sörgel, M., Botía, S., Acevedo, O., et al. (2021). A case study of a gravity wave induced by Amazon forest orography and low level jet generation. *Agricultural and Forest Meteorology*, *307*, 108457. https://doi.org/10.1016/j.agrformet.2021.108457

Corsmeier, U., Kalthoff, N., Kolle, O., Kotzian, M., & Fiedler, F. (1997). Ozone concentration jump in the stable nocturnal boundary layer during a LLJ-event. *Atmospheric Environment*, *31*(13), 1977–1989. https://doi.org/10.1016/S1352-2310(96)00358-5

de Jesus, E. M., Rocha, R. P., Reboita, M. S., Llopart, M., Dutra, L. M. M., & Remedio, A. R. C. (2016). Contribution of cold fronts to seasonal rainfall in simulations over the southern la Plata Basin. *Climate Research*, *68*(2–3), 243–255. https://doi.org/10.3354/cr01358

Dominutti, P., Nogueira, T., Borbon, A., Andrade, M. D. F., & Fornaro, A. (2016). One-year of NMHCs hourly observations in São Paulo megacity: Meteorological and traffic emissions effects in a large ethanol burning context. *Atmospheric Environment*, *142*, 371–382. https://doi.org/10.1016/j.atmosenv.2016.08.008

Du, Y., Qinghong, Z., Chen, Y.-L., Zhao, Y., & Wang, X. (2014). Numerical simulations of spatial distributions and diurnal variations of low-level jets in China during early summer. *Journal of Climate*, *27*(2010), 5747–5767. https://doi.org/10.1175/JCLI-D-13-00571.1

Duarte, H. F., Leclerc, M. Y., & Zhang, G. (2012). Assessing the shear-sheltering theory applied to low-level jets in the nocturnal stable boundary layer. *Theoretical and Applied Climatology*, *110*(3), 359–371. https://doi.org/10.1007/s00704-012-0621-2

Emeis, S. (2014a). Current issues in wind energy meteorology. *Meteorological Applications*, *21*(4), 803–819. https://doi.org/10.1002/met.1472

Emeis, S. (2014b). Wind speed and shear associated with low-level jets over Northern Germany. *Meteorologische Zeitschrift*, *23*(3), 295–304. https://doi.org/10.1127/0941-2948/2014/0551

Furlan, C., Oliveira, A. P., Soares, J., Codato, G., & Escobedo, J. F. (2012). The role of clouds in improving the regression model for hourly values of diffuse solar radiation. *Applied Energy*, *92*, 240–254. https://doi.org/10.1016/j.apenergy.2011.10.032

Garreaud, R. D., & Muñoz, R. C. (2005). The low-level jet off the west coast of subtropical South America: Structure and variability. *Monthly Weather Review*, *133*(8), 2246–2261. https://doi.org/10.1175/MWR2972.1

González-Rodríguez, L., Oliveira, A. P., Rodríguez-López, L., Rosas, J., Contreras, D., & Baeza, A. C. (2021). A study of UVER in Santiago, Chile based on long-term in situ measurements (five years) and empirical modelling. *Energies*, *14*(2), 368. https://doi.org/10.3390/en14020368

He, M.-Y., Liu, H.-B., Wang, B., & Zhang, D.-L. (2016). A modeling study of a low-level jet along the Yun-Gui Plateau in south China. *Journal of Applied Meteorology and Climatology*, *55*(1), 41–60. https://doi.org/10.1175/JAMC-D-15-0067.1

Higgins, R. W., Yao, Y., Yarosh, E. S., Janowiak, J. E., & Mo, K. C. (1997). Influence of the Great Plains low-level jet on summertime precipitation and moisture transport over the central United States. *Journal of Climate*, *10*(3), 481–507. https://doi.org/10.1175/1520-0442(1997)010<0481:iotgpl>2.0.co;2

Holton, J. R. (1967). The diurnal boundary layer wind oscillation above sloping terrain. *Tellus*, *19*(2), 199–205. https://doi.org/10.3402/tellusa.v19i2.9766

Hu, X.-M., Klein, P. M., Xue, M., Lundquist, J. K., Zhang, F., & Qi, Y. (2013). Impact of low-level jets on the nocturnal urban heat island intensity in Oklahoma City. *Journal of Applied Meteorology and Climatology*, *52*(8), 1779–1802. https://doi.org/10.1175/JAMC-D-12-0256.1

Hu, X.-M., Klein, P. M., Xue, M., Zhang, F., Doughty, D. C., Forkel, R., & Fuentes, J. D. (2013). Impact of the vertical mixing induced by low-level jets on boundary layer ozone concentration. *Atmospheric Environment*, *70*, 123–130. https://doi.org/10.1016/j.atmosenv.2012.12.046

Iago, A., Eiras-Barca, J., Nieto, R., & Gimeno, L. (2019). Global climatology of nocturnal low-level jets and associated moisture sources and sinks. *Atmospheric Research*, *229*, 39–59. https://doi.org/10.1016/j.atmosres.2019.06.016

IBGE. (2019). IBGE demographics censuses. Retrieved from https://ibge.gov.br/

Jones, C. (2019). Recent changes in the South America low-level jet. *Climate and Atmospheric Science*, *2*(1), 1–8. https://doi.org/10.1038/s41612-019-0077-5

Kallistratova, M., Kouznetsov, R. D., Kuznetsov, D., Kuznetsova, I. N., Nakhaev, M., & Chirokova, G. (2009). Summertime low-level jet characteristics measured by sodars over rural and urban areas. *Meteorologische Zeitschrift*, *18*(3), 289–295. https://doi.org/10.1127/0941-2948/2009/0380

Kallistratova, M. A., & Kouznetsov, R. D. (2012). Low-level jets in the Moscow region in summer and winter observed with a sodar network. *Boundary-Layer Meteorology*, *143*(1), 159–175. https://doi.org/10.1007/s10546-011-9639-8

Karam, H. A. (2002). *Estudo do Jato de Baixos Níveis de Iperó e das Implicações no Transporte de Poluentes no Estado de São Paulo (Doctoral Thesis)*. Institute of Astronomy, Geophysics and Atmospheric Sciences. Retrieved from https://www.teses.usp.br/teses/disponiveis/14/14133/tde-29052003-161622/pt-br.php

Karipot, A., Leclerc, M. Y., & Zhang, G. (2009). Characteristics of nocturnal low-level jets observed in the north Florida area. *Monthly Weather Review*, *137*(8), 2605–2621. https://doi.org/10.1175/2009MWR2705.1

King, J. C., Lachlan-Cope, T. A., Ladkin, R. S., & Weiss, A. (2008). Airborne measurements in the stable boundary layer over the Larsen Ice Shelf, Antarctica. *Boundary-Layer Meteorology*, *127*(3), 413–428. https://doi.org/10.1007/s10546-008-9271-4

Klein, P. M., Hu, X. M., Shapiro, A., & Xue, M. (2016). Linkages between boundary-layer structure and the development of nocturnal low-level jets in central Oklahoma. *Boundary-Layer Meteorology*, *158*(3), 383–408. https://doi.org/10.1007/s10546-015-0097-6

Klein, P. M., Hu, X. M., & Xue, M. (2014). Impacts of mixing processes in nocturnal atmospheric boundary layer on urban ozone concentrations. *Boundary-Layer Meteorology*, *150*(1), 107–130. https://doi.org/10.1007/s10546-013-9864-4

Kutsher, J., Haikin, N., Sharon, A., & Heifetz, E. (2012). On the formation of an elevated nocturnal inversion layer in the presence of a low-level jet: A case study. *Boundary-Layer Meteorology*, *144*(3), 441–449. https://doi.org/10.1007/s10546-012-9720-y

Li, D., Storch, H. V., Yin, B., Xu, Z., Qi, J., Wei, W., & Guo, D. (2018). Low-level jets over the Bohai Sea and Yellow Sea: Climatology, variability, and the relationship with regional atmospheric circulations. *Journal of Geophysical Research: Atmospheres*, *123*(10), 5240–5260. https://doi.org/10.1029/2017JD027949

Li, J., & Chen, Y.-L. (1998). Barrier jets during TAMEX. *Monthly Weather Review*, *126*(4), 959–971. https://doi.org/10.1175/1520-0493(1998)126<0959:BJDT>2.0.CO;2

Lundquist, J. K. (2003). Intermittent and elliptical inertial oscillations in the atmospheric boundary layer. *Journal of the Atmospheric Sciences*, *60*(21), 2661–2673. https://doi.org/10.1175/1520-0469(2003)060<2661:iaeioi>2.0.co;2

Lundquist, J. K., & Mirocha, J. D. (2008). Interaction of nocturnal low-level jets with urban geometries as seen in Joint Urban 2003 data. *Journal of Applied Meteorology and Climatology*, *47*(1), 44–58. https://doi.org/10.1175/2007JAMC1581.1

Marengo, J. A., Soares, W. R., Saulo, C., & Nicolini, M. (2004). Climatology of the low-level jet east of the Andes as derived from the NCEP-NCAR reanalyses: Characteristics and temporal variability. *Journal of Climate*, *17*(12), 2261–2280. https://doi.org/10.1175/1520-0442(2004)017<2261:cotlje>2.0.co;2

Markowski, P., & Richardson, Y. (2011). *Mesoscale meteorology in midlatitudes*. John Wiley and Sons.

Martins, H. S., Sá, L. D. A., & Moraes, O. L. L. (2013). Low level jets in the pantanal wetland nocturnal boundary layer—Case studies. *American Journal of Environmental Engineering*, *3*(1), 32–47. https://doi.org/10.5923/j.ajee.20130301.06

Miao, Y., Guo, J., Liu, S., Wei, W., Zhang, G., Lin, Y., & Zhai, P. (2018). The climatology of low-level jet in Beijing and Guangzhou, China. *Journal of Geophysical Research: Atmospheres*, *123*(5), 2816–2830. https://doi.org/10.1002/2017JD027321

Miao, Y., Liu, S., Sheng, L., Huang, S., & Li, J. (2019). Influence of boundary layer structure and low-level jet on PM2.5 pollution in Beijing: A case study. *International Journal of Environmental Research and Public Health*, *16*(4), 616. https://doi.org/10.3390/ijerph16040616

Montini, T. L., Jones, C., & Carvalho, L. M. V. (2019). The South American low-level jet: A new climatology, variability, and changes. *Journal of Geophysical Research: Atmospheres*, *124*(3), 1200–1218. https://doi.org/10.1029/2018JD029634

Nair, K. N., Freitas, E. D., Sánchez-Ccoyllo, O. R., Silva Dias, M. A. F., Silva Dias, P. L., Andrade, M. F., & Massambani, O. (2004). Dynamics of urban boundary layer over São Paulo associated with mesoscale processes. *Meteorology and Atmospheric Physics*, *86*(1–2), 87–98. https://doi.org/10.1007/s00703-003-0617-7

Oliveira, A. P., Bornstein, R. D., & Soares, J. (2003). Annual and diurnal wind patterns in the city of São Paulo. *Water, Air, and Soil Pollution: Focus*, *3*(5/6), 3–15. https://doi.org/10.1023/A:1026090103764

Oliveira, A. P., & Fitzjarrald, D. R. (1994). The Amazon river breeze and local boundary layer: I. Linear analysis and modelling. *Boundary-Layer Meteorology*, *67*, 75–96.

Oliveira, A. P., Marques Filho, E. P., Ferreira, M. J., Codato, G., Ribeiro, F. N. D., Landulfo, E., et al. (2020). Assessing urban effects on the climate of metropolitan regions of Brazil—Preliminary results of the MCITY BRAZIL project. *Exploratory Environmental Science Research*, *1*(1), 38–77. https://doi.org/10.47204/EESR.1.1.2020.038-077

Parish, T. R. (1982). Barrier winds along the Sierra Nevada mountains. *Journal of Applied Meteorology*, *21*(7), 925–930. https://doi.org/10.1175/1520-0450(1982)021<0925:bwatsn>2.0.co;2

Parish, T. R. (2000). Forcing of the summertime low-level jet along the California coast. *Journal of Applied Meteorology*, *39*(12), 2421–2433. https://doi.org/10.1175/1520-0450(2000)039<2421:FOTSLL>2.0.CO;2

Parish, T. R. (2017). On the forcing of the summertime Great Plains low-level jet. *Journal of the Atmospheric Sciences*, *74*(12), 3937–3953. https://doi.org/10.1175/JAS-D-17-0059.1

Ribeiro, F. N. D., Oliveira, A. P., Soares, J., Miranda, R. M., Barlage, M., & Chen, F. (2018). Effect of sea breeze propagation on the urban boundary layer of the metropolitan region of Sao Paulo, Brazil. *Atmospheric Research*, *214*, 174–188. https://doi.org/10.1016/j.atmosres.2018.07.015

Ribeiro, F. N. D., Soares, J., & Oliveira, A. P. (2016). Sea-Breeze and topographic influences on the planetary boundary layer in the coastal upwelling area of Cabo Frio (Brazil). *Boundary-Layer Meteorology*, *158*(1), 139–150. https://doi.org/10.1007/s10546-015-0085-x

Roy, S., Sentchev, A., Schmitt, F. G., Augustin, P., & Fourmentin, M. (2021). Waves on turbulent motions and energy fluxes in the lower atmospheric boundary layer. *Boundary-Layer Meteorology*, *180*(3), 527–542. https://doi.org/10.1007/s10546-021-00629-x

Ruchith, R. D., & Raj, P. E. (2015). Features of nocturnal low level jet (NLLJ) observed over a tropical Indian station using high resolution Doppler wind lidar. *Journal of Atmospheric and Solar-Terrestrial Physics*, *123*, 113–123. https://doi.org/10.1016/j.jastp.2015.01.001

Ruchith, R. D., Raj, P. E., Kalapureddy, M. C. R., Deshpande, S. M., & Dani, K. K. (2014). Time evolution of monsoon low-level jet observed over an Indian tropical station during the peak monsoon period from high-resolution Doppler wind lidar measurements. *Journal of Geophysical Research: Atmospheres*, *119*(4), 1786–1795. https://doi.org/10.1002/2013JD020752

Sánchez, M. P., Oliveira, A. P., Varona, R. P., Tito, J. V., Codato, G., Ribeiro, F. N. D., et al. (2020). Radiosonde based analysis of the urban boundary layer in the metropolitan region of São Paulo, Brazil. *Earth and Space Science*, *7*(2), e2019EA000781. https://doi.org/10.1029/2019EA000781

Shapiro, A., Fedorovich, E., & Rahimi, S. (2016). A unified theory for the Great Plains nocturnal low-level jet. *Journal of the Atmospheric Sciences*, *73*(8), 3037–3057. https://doi.org/10.1175/JAS-D-15-0307.1

Smedman, A. S., Högström, U., & Hunt, J. C. R. (2004). Effects of shear sheltering in a stable atmospheric boundary layer with strong shear. *Quarterly Journal of the Royal Meteorological Society*, *130*(596), 31–50. https://doi.org/10.1256/qj.03.68

Song, J., Liao, K., Coulter, R. L., & Lesht, B. M. (2005). Climatology of the low-level jet at the southern Great Plains atmospheric boundary layer experiments site. *Journal of Applied Meteorology*, *44*(10), 1593–1606. https://doi.org/10.1175/jam2294.1

Stull, R. B. (1988). *An introduction to boundary layer meteorology*. Kluwer Academic Publishers.

Sullivan, J. T., Rabenhorst, S. D., Dreessen, J., Mcgee, T. J., Delgado, R., Twigg, L., & Sumnicht, G. (2017). Lidar observations revealing transport of O_3 in the presence of a nocturnal low-level jet: Regional implications for "next-day" pollution. *Atmospheric Environment*, *158*, 160–171. https://doi.org/10.1016/j.atmosenv.2017.03.039

Trier, S. B., Christopher, A. D., & Carbone, R. E. (2014). Mechanisms governing the persistence and diurnal cycle of a heavy rainfall corridor. *Journal of the Atmospheric Sciences*, *71*(11), 4102–4126. https://doi.org/10.1175/JAS-D-14-0134.1

Van de Wiel, B. J. H., Moene, A. F., Steeneveld, G. J., Baas, P., Bolveld, F. C., & Holtslag, A. A. M. (2010). A conceptual view on inertial oscillations and nocturnal low-level jets. *Journal of the Atmospheric Sciences*, *67*(8), 2679–2689. https://doi.org/10.1175/2010JAS3289.1

Vemado, F., & Pereira Filho, A. J. (2016). Severe weather caused by heat island and sea breeze effects in the metropolitan area of São Paulo, Brazil. *Advances in Meteorology*, 8364134–8364213. https://doi.org/10.1155/2016/8364134

Wang, Y., Klipp, C. L., Garvey, D. M., Ligon, D. A., Williamson, C. C., Chang, S. S., et al. (2007). Nocturnal low-level-jet-dominated atmospheric boundary layer observed by a Doppler lidar over Oklahoma City during JU2003. *Journal of Applied Meteorology and Climatology*, *46*(12), 2098–2109. https://doi.org/10.1175/2006JAMC1283.1

Wei, W., Wu, B. G., Ye, X. X., Wang, H. X., & Zhang, H. S. (2013). Characteristics and mechanisms of low-level jets in the Yangtze River Delta of China. *Boundary-Layer Meteorology*, *149*(3), 403–424. https://doi.org/10.1007/s10546-013-9852-8

Wei, W., Zhang, H. S., Ye, X. X., Chakravarty, K., & Goswami, B. N. (2014). Comparison of low-level jets along the north coast of China in summer. *Journal of Geophysical Research: Atmospheres*, *119*(10), 9692–9706. https://doi.org/10.1002/2014JD021606

Whiteman, C. D., Bian, X., & Zhong, S. (1997). Low-level jet climatology from enhanced rawinsonde observations at a site in the southern Great Plains. *Journal of Applied Meteorology*, *36*(10), 1363–1376. https://doi.org/10.1175/1520-0450(1997)036<1363:lljcfe>2.0.co;2

Wittich, K. P., Hartmann, J., & Roth, R. (1986). On nocturnal wind shear with a view to engineering applications. *Boundary-Layer Meteorology*, *37*(3), 215–227. https://doi.org/10.1007/BF00122985

Zhang, Y., Guo, J., Yang, Y., Wang, Y., & Yim, S. H. L. (2020). Vertical wind shear modulates particulate matter pollution: A perspective from radar wind profiler observations in Beijing, China. *Remote Sensing*, *12*(3), 546. https://doi.org/10.3390/rs12030546

Zhang, Y., Xue, M., Zhu, K., & Zhou, B. (2019). What is the main cause of diurnal variation and nocturnal peak of summer precipitation in sichuan basin, Chinas? The key role of boundary layer low-level jet inertial oscillations. *Journal of Geophysical Research: Atmospheres*, *124*(5), 2643–2664. https://doi.org/10.1029/2018JD029834

Erratum

The following errors were discovered after publication of this paper: In Tables 1–3, several values were incorrectly typeset. These errors have been corrected, and this may be considered the authoritative version of record.